Metabolic reprogramming of hypoxic tumour-associated macrophages through CSF-1R targeting favours treatment efficiency in colorectal cancers

Khaldoun Gharzeddine[1], Cristina Gonzales Pietro[1], Marie Malier[1], Clara Hennot[1], Renata Grespan[1], Yoshiki Yamaryo-Botté[2], Cyrille Y. Botté[2], Fabienne Thomas[3], Marie-Hélène Laverriere[1,4], Edouard Girard[5], Gael Roth[1,6], Arnaud Millet[1,6]

1. Univ.Grenoble Alpes, Inserm U1209, CNRS UMR5309, Institute for Advanced Biosciences, Team Mechanobiology, Immunity and Cancer, 38000 Grenoble, France

2. Univ.Grenoble Alpes, Inserm U1209, CNRS UMR5309, Institute for Advanced Biosciences, Apicolipid Team & Gemeli metabolomic platform, 38000 Grenoble, France

3. Centre de Recherches en Cancérologie, Inserm, CNRS, Université Toulouse III-Paul Sabatier and IUCT-Oncopole, Toulouse, France.

4. Univ.Grenoble Alpes, CNRS, CHU Grenoble Alpes pathology department, TIMC, 38000 Grenoble, France

5. Univ.Grenoble Alpes, CHU Grenoble Alpes digestive and emergency surgery department, 38000 Grenoble, France

6. Univ.Grenoble Alpes, CHU Grenoble Alpes hepatogastroenterology department, 38000 Grenoble, France

Running title: Metabolic reprogramming of macrophages through CSF-1R targeting

Keywords: CSF-1R antagonists, Cholesterol, Hypoxia, Tumor-Associated Macrophages, Chemoresistance.

Corresponding author: Arnaud Millet MD PhD,

e-mail: arnaud.millet@inserm.fr

Team Mechanobiology, Immunity and Cancer, Institute for Advanced Biosciences

Building Albert Bonniot

Boulevard de la Chantourne

38700 La Tronche

France

The authors declare no conflicts of interest.

Abstract

Tumour associated macrophages participate to the complex sustainability network that favours tumour growth. Among the various strategies that have been developed to target these cells, CSF-1R receptor blockade is one of the most promising one. Here, we characterize the resulting state of human macrophages exposed to a CSF-1R kinase inhibitor. We find that inhibition of CSF-1R receptor in human macrophages is able to impair cholesterol synthesis, fatty acid metabolism and hypoxia-driven expression of dihydropyrimidine dehydrogenase, an enzyme responsible for the 5-FU macrophage-mediated chemoresistance. We demonstrate that this inhibition of the CSF-1R receptor leads to a downregulation of the expression of SREBP2, a transcription factor controlling the cholesterol and fatty acid synthesis. We also demonstrate that the inhibition of ERK1/2 phosphorylation resulting from the CSF-1R receptor targeting destabilizes the expression of HIF2α in hypoxia resulting in the downregulation of dihydropyrimidine dehydrogenase expression restoring the sensitivity to 5-Fluorouracil in colorectal cancers. These results reveal the unexpected metabolic rewiring resulting from the CSF-1R receptor targeting of human macrophages in tumours.

54 **Introduction**

55 A large body of work has been reported providing compelling evidence that tumour-
56 associated macrophages (TAMs) participate to tumour growth, treatment resistance and
57 metastasis (DeNardo & Ruffell, 2019; Engblom *et al*, 2016). Indeed, TAMs are associated with
58 bad prognosis in a vast majority of solid tumours (Cortese *et al*, 2020). Consequently, a huge
59 effort has been done to target TAMs in order to direct the immune response against the
60 tumour (Mantovani *et al*, 2022). CSF-1R is a receptor, possessing an intrinsic tyrosine kinase
61 activity, which recognizes CSF-1 (M-CSF, macrophage colony stimulating factor) and IL-34.
62 CSF-1/CSF-1R (CSF-1 receptor) signalling pathway is involved in the survival, proliferation,
63 differentiation and chemotaxis of macrophages (Stanley & Chitu, 2014). This pivotal role
64 opens the way to use CSF-1R receptor targeting in various pathological contexts and especially
65 in cancer to modulate macrophages (Cannarile *et al*, 2017). CSF-1R receptor targeting has
66 been used in various tumour mice models reaching promising results but only mild beneficial
67 effects in humans when used alone (Mantovani *et al*, 2022). Moreover, the recognition that
68 the type of tumour model used (O'Brien *et al*, 2021) and the modification of the cellular
69 environment such as oxygen availability (Pradel *et al*, 2016) impact the efficiency of the CSF-
70 1R targeting highlights the need for a better understanding of the CSF-1R receptor targeting's
71 functional consequences on human macrophages.

72 The importance of CSF-1R receptor blockade beyond apoptosis induction has been recognized
73 in animal models advocating for the opportunity to attain an anti-tumour phenotypic
74 reprogramming (Pyonteck *et al*, 2013). Nevertheless, the mechanisms involved in
75 macrophage's reprogramming through CSF-1R targeting are unclear.

76 Here, we characterize the functional consequences of CSF-1R receptor inhibitors on human
77 macrophages. We show that inhibition of CSF-1R receptor is associated with an impairment
78 of cholesterol and fatty acids synthesis under the control of the transcription factor SREBP2.
79 Moreover, CSF-1R receptor blockade leads to an inhibition of the phosphorylated state of
80 ERK1/2 resulting in the decrease of HIF2α, a hypoxic response transcription factor,
81 expression. A consequence of the HIF2α-dependent hypoxic response is the downregulation
82 of dihydropyrimidine dehydrogenase expression, the limiting rate enzyme of the first step of
83 the pyrimidine catabolism pathway, which is responsible for a hypoxia driven macrophage-
84 mediated chemoresistance against 5-Fluorouracil in colorectal cancers (Malier *et al*, 2021).

85 **Results**

86 **Complete CSF-1R inhibition is associated with a profound phenotypic change without death**
87 **induction in human macrophages**

88 Upon ligation of CSF-1, the CSF-1 receptor dimerizes leading to multiple site phosphorylation
89 of the intracellular tail of the receptor (Stanley & Chitu, 2014). To study the resulting effect of
90 CSF-1R receptor dependent signalling pathway inhibition, we first evaluated the response of
91 the phosphorylation of the tyrosine 723 to an increasing dose of edicotinib, a tyrosine kinase
92 inhibitor specific to CSF-1R. We found that edicotinib at 10µM is able to completely inhibit
93 CSF-1R's phosphorylation (Figure 1A). CSF-1R receptor targeting by tyrosine kinase inhibitors
94 is a strategy used in mice to deplete macrophages (Ries *et al*, 2014). Nevertheless, we found
95 that the complete inhibition of the phosphorylation of CSF-1R in human primary macrophages
96 was not associated with cell death induction (7AAD and Annexin V) (Figure 1B & Supplemental
97 Figure 1) or disruption of cellular metabolic activity (MTT) (Figure 1C). The importance of CSF-
98 1 in macrophages differentiation and polarisation lead us to evaluate precisely the impact of

99 CSF-1R receptor blockade on human macrophage phenotype. To attain this goal, we
100 performed a global gene expression analysis using RNA sequencing (RNAseq) on bulk
101 macrophages 48h after exposition to vehicle and edicotinib. To extract differentially
102 expressed genes between treated and naïve macrophages, we used a moderated t-test with
103 an adjusted p-value (Benjamini-Hochberg procedure with a threshold set at q-value <0.05)
104 and a threshold for the fold change set at 2 (log_2 FC <-1 or Log_2 FC > 1). CSF-1R receptor
105 inhibition by edicotinib was associated with 740 downregulated and 481 upregulated genes
106 (Figure 1D). We then used a Gene Ontology (GO) enrichment analysis to identify pathways
107 affected by edicotinib. The GO terms associated with genes downregulated by edicotinib
108 indicates that the regulation of the cholesterol metabolic pathway, the inhibition of the
109 ERK1/2 pathway, and lipid synthesis are the main of biological processes identified resulting
110 from the blockade of CSF-1R receptor (Figure 1E).

111 **CSF-1/CSF-1R controls cholesterol synthesis in human macrophages via the transcription**
112 **factor SREBP2**

113 To explore the gene ontology identification of cholesterol synthesis regulation under CSF-1R
114 targeting, we studied the expression of all the enzymes involved in the cholesterol synthesis
115 starting from acetyl-CoA. Cholesterol, an essential lipid component of mammalian cell, is
116 mainly obtained via endogenous synthesis or uptake. The endogenous synthesis relies on
117 nearly 30 enzymatic reactions (Nes, 2011). We found that genes coding for enzymes involved
118 in cholesterol synthesis *ACAT2*, *HMGCS1, HMGCR, MVK, PMVK, MVD, IDI1, FDPS, FDFT1,*
119 *SQLE, LSS, CYP15A1, TMF7SF2, NSDHL, HSD17B7, MSMO1, SC5D, EBP, DCHR7, DCHR24* are
120 downregulated under edicotonib exposure (Figure 2A) and apart two of them (*PMVK*, *LSS*) the
121 fold change is greater than 2 (Figure 2B). The control of cholesterol synthesis genes by the

122 CSF-1/CSF-1R pathway was confirmed by the stimulation of human macrophages by CSF-1
123 showing the upregulation of *HMGCR* and *DHCR7* (Figure 2C). SREBP2 (Sterol regulatory
124 element-binding protein 2) is a helix-loop-helix leucine zipper transcription factor that
125 regulates the synthesis and cellular uptake of cholesterol (Horton *et al*, 1998). Using the
126 ENCODE data set (The ENCODE (ENCyclopedia Of DNA Elements) Project, 2004), we have
127 explored the known targets of this transcription factor and found that the cholesterol
128 synthesis genes are under SREBP2 control (Figure 2D). Interestingly, the LDL receptor (*LDLR*)
129 which is responsible for cellular uptake of cholesterol from the extracellular milieu and the
130 fatty acid synthetase (*FASN*) are also SREBP2 targets genes (Figure 2D). We validated the
131 SREBP2 dependent expression of cholesterol synthesis genes (*HMGCR*, *DHRC7*) and *LDLR*
132 using RNAi targeting against SREBF2, the gene coding for SREBP2 protein (Figure 2E). We
133 demonstrated the control of *SREBF2* by the CSF-1/CSF-1R pathway by showing that *SREBF2*
134 expression is increased under CSF-1 stimulation (Figure 2F) and decreased when CSF-1R is
135 blocked by edicotinib (Figure 2G). We confirmed that the nuclear active form of SREBP2
136 expression is downregulated by the CSF-1R blockade (Figure 2H). Moreover, *LDLR*, a SREBP2
137 target, is downregulated by edicotinib (Figure 2I). We observed the resulting decrease of
138 cellular cholesterol amount under the exposure to edicotinib similarly to what is found using
139 RNAi targeting of SREBF2 or blockade of HMGCR activity with simvastatin, a specific inhibitor
140 (Figure 2J). The cholesterol cellular homeostasis is a balance between synthesis, uptake and
141 efflux. The impairment of cholesterol synthesis and uptake by CSF-1R receptor blockade could
142 be compensated by a decrease in cholesterol efflux. To appreciate this possibility, we studied
143 the expression of the two main cholesterol efflux transporters expressed in macrophages
144 ABCA1 and ABCG1. We found that the CSF-1R targeting does not decrease the expression of
145 these transporters in macrophages (Supplemental Figure 2A).Furthermore, we found that the

146 decrease of intracellular cholesterol amount, induced by CSF-1R receptor blockade, resulted
147 in a global decrease of secreted cholesterol by macrophages (Supplemental Figure 2B).

148 **Edicotinib interferes with the macrophage - tumour communication resulting in cholesterol**
149 **synthesis modulation in colorectal cancers**

150 Membrane cholesterol efflux from macrophages has been reported to participate to tumour
151 growth (Goossens *et al*, 2019). This efflux relies on the ability of macrophages to express efflux
152 transporters but also on the maintenance of their intracellular cholesterol pool based on
153 synthesis and uptake. To further understand the importance of cholesterol synthesis in the
154 cross-talk between macrophages and tumours, we performed a co-culture between human
155 macrophages and tumorous or non tumorous tissues from the same colon obtained from
156 surgical of colorectal adenocarcinomas (Figure 2K). We observed that macrophages under the
157 influence of tumorous tissues upregulate their cholesterol synthesis genes as well as the
158 cholesterol uptake receptor LDLR under the control of SREBF2 which is upregulated by the
159 tumour (Figure 2L). We also demonstrated that edicotinib is able to counter this metabolic
160 reprogramming driven by the tumour by interfering with the induction of synthesis and
161 uptake of cholesterol (Figure 2L). This communication between tumours and macrophages
162 suggested the involvement of the CSF-1/CSF-1R pathway. We confirmed that tumours secrete
163 significantly more CSF-1 than non-tumorous tissues driving the cholesterol synthesis and
164 uptake in macrophages (Figure 2M). Nevertheless, we sought to verify if edicotinib could also
165 impair the expression of the CSF-1R receptor at the surface of macrophages but found no
166 decrease in the expression of the receptor following CSF-1R blockade (Figure 2N). We
167 interestingly found that the ability of macrophages to produce their own CSF-1 is impaired in
168 human macrophages exposed to edicotinib (Figure 2O). Even if tumours do not increase the

169 autocrine associated production in macrophages, edicotinib is able to downregulate this
170 production in macrophages reinforcing the blockade of the CSF-1/CSF-1R pathway (Figure 2P).

171 **CSF-1R receptor targeting downregulates HIF2α expression in hypoxia through ERK1/2**
172 **phosphorylation inhibition**

173 Previous studies revealed that some environmental factors could modulate the cellular
174 response to CSF-1R receptor targeting (Pradel *et al*, 2016). Among these factors, hypoxia is of
175 particular interest as the tumour environment is associated with low oxygen availability
176 (Wilson & Hay, 2011). To assess the interplay between hypoxia and CSF-1R receptor targeting,
177 we performed the study of differentially expressed genes in hypoxia compared to normoxia
178 and analysed the impact of edicotinib on the hypoxic response (Figure 3A), CSF-1R receptor
179 blockade's cell survival profile in hypoxia was similar to what we found in normoxia
180 (Supplemental Figure 3A). The heat-map analysis revealed that specific hypoxic sensitive
181 genes present two different patterns: specific hypoxic sensitive genes that maintain their
182 expression profile under CSF-1R receptor blockade (clusters 1 & 3) and genes with a modified
183 profile with CSF-1R receptor blockade (clusters 2, 4 & 5). Among hypoxia upregulated genes
184 (cluster 3), we found multiple genes *LDHA*, *NDRG1*, *P4HA1* and *SLC2A1* (Figure 3B), which are
185 part of HIF1α target genes set identified by ChIP enrichment analysis (Lachmann *et al*, 2010)
186 suggesting that the HIF1α-dependent hypoxic response is mainly independent of the CSF-1R
187 pathway. Of particular interest, we observed that the downregulation of some hypoxic genes
188 is abolished by CSF-1R receptor blockade (cluster 2) with an increased expression profile in
189 normoxia (Figure 3A). *EPAS1* is one of these genes (Figure 3C). *EPAS1* gene codes for the
190 transcription factor HIF-2α, which plays an essential role in the cellular response to low
191 oxygen environment (McGettrick & O'Neill, 2020). The downregulation of *EPAS1* mRNA in

192 hypoxia contrasts with the stabilisation of the protein HIF-2α in the same condition (Figure
193 3D). To understand the role of CSF-1R in the HIF-2α dependent hypoxic response, we sought
194 to clarify HIF-2α function by studying *FLT1* (VEGFR1), a HIF-2α target gene. Indeed, *FLT1*
195 expression is increased in hypoxic macrophages (Figure 3E) under the control of HIF-2α
196 transcriptional activity as RNAi targeting of EPAS1 in hypoxic macrophages demonstrates it
197 (Supplemental Figure 3B). The decrease of FLT1 (Figure 3E) and the corresponding increase
198 of EPAS1 mRNA level with CSF-1R receptor blockade by edicotinib in hypoxic macrophages
199 (Figure 3C) advocates for a decrease of HIF-2α expression in hypoxia under CSF-1R receptor
200 blockade, a pattern that we confirmed by immunoblot (Figure 3F). Interestingly, the activation
201 of HIF-2α leading to its migration to the nucleus and its fixation on HRE (Hypoxic Response
202 Elements) genes promotors is ERK1/2 dependent (Conrad *et al*, 1999). The identification of
203 the ERK1/2 pathway as a target of CSF-1R blockade in normoxia (Figure 1E) suggested the
204 possibility of a similar pattern in hypoxia. Effectively, we confirmed that pattern by a gene set
205 enrichment analysis (GSEA) (Figure 3G) and by immunoblot of phosphorylated sites p-ERK1/2
206 in hypoxia (Figure 3H). The inhibition of ERK1/2 with the MEK1 inhibitor U0126 was able to
207 downregulate the expression of HIF-2α similarly to what is observed with edicotinib (Figure
208 3I). Moreover, HIF-2α protein expression is a direct sensor of oxygen availability
209 intracellularly. Oxygen diffusion from the cellular environment into the cell is mainly
210 controlled by the plasma membrane permeability which is profoundly affected by the
211 membrane concentration of cholesterol (Dotson *et al*, 2017). Decrease of cholesterol at the
212 membrane will favour oxygen diffusion into the cell. Therefore, the decrease of cholesterol
213 synthesis induced by CSF2R blockade suggested a complementary involvement of the cellular
214 cholesterol in HIF-2α expression. Indeed, the RNAi targeting of SREBF2 leading to the
215 decrease of cholesterol synthesis and cellular uptake showed a small decrease of HIF-2α

216 (Figure 3J) suggesting a potential combined effect between SREBF2 and ERK1/2 dependent
217 processes. The study of the expression of cholesterol synthesis genes (*HMGCR*, *DHCR7*) and
218 cellular uptake (*LDLR*) confirms that these two mechanisms are independent as ERK1/2
219 inhibition did not downregulate these genes contrary to edicotinib exposure (Supplemental
220 Figure 3C).

221 **Increase of fatty acid synthesis in hypoxia is reversed by CSF-1R targeting in human**
222 **macrophages**

223 The recent recognition that hypoxia activates SREBP2 in hypoxic THP1-monocytes raised the
224 possibility that CSF-1R receptor blockade ability to dampen cholesterol synthesis could be
225 antagonized in hypoxic macrophages (Nakahara *et al*, 2023). Nevertheless, these authors
226 reported a small if not inexistent effect in hypoxic differentiated THP1-macrophages
227 (Nakahara *et al*, 2023). We sought to clarify this issue in our primary human macrophages.
228 The study of differentially repressed genes in hypoxic macrophages exposed confirmed the
229 results obtained in normoxia with a downregulation of the cholesterol synthesis and of
230 ERK1/2 pathway under CSF-1R blockade (Figure 4A). Along with the cholesterol synthesis and
231 cellular uptake under the control of *SREBF2*, we observed that *SREBF1* and *FASN* were
232 similarly down regulated in hypoxia under CSF-1R blockade (Figure 4B). SREBP1, the
233 transcription factor coded by *SREBF1* gene, is involved in fatty acid synthesis and fatty acid
234 synthetase (FASN) is under the control of SREBPs transcription factors. Furthermore, the
235 analysis of the hypoxic specific response genes modulated by edicotinib (cluster 4 in Figure
236 3A) revealed that lipid transport, localization is associated with the hypoxic response (Figure
237 4C), and that this response could be disrupted by CSF-1R blockade. *FASN*, a gene under the
238 control of *SREBF1* and *SREBF2*, is the main enzymatic complex responsible for the synthesis

239 of palmitic acid (C16:0) and stearic acid (C18:0) from malonyl-CoA subsequently transformed
240 in palmitoleic acid (C16:1 cis) and oleic acid (C18:1 cis) respectively (Figure 4D). Fatty acids,
241 notably oleic acid, have been involved in the macrophage commitment toward an
242 immunosuppressive $CD206^{+}CD38^{+}$ phenotype in tumour associated macrophages (Wu *et al*,
243 2019). Using gas chromatography mass spectrometry methodology (GC-MS), we confirmed
244 the significant increase of these fatty acids in hypoxic macrophages and the ability of the CSF-
245 1R blockade to dampen that synthesis (Figure 4E). We also confirmed downregulation of
246 CD206 expression in tumour-educated macrophages (Figure 4F & Supplemental Figure 4A)
247 and *CD206*, *CD38* genes expression in hypoxic macrophages exposed to edicotinib
248 (Supplemental Figure 4 B). We also found that FASN inhibition by a specific inhibitor (C75) in
249 hypoxic macrophages is sufficient to prevent CD206 expression driven by IL-4 (Figure 4G).
250 These results advocate for a fatty acid synthase mediated inhibition of CD206 following CSF-
251 1R targeting.

252 **CSF-1R targeting downregulates the expression of dihydropyrimidine dehydrogenase**
253 **preventing 5-FU hypoxic macrophage-driven chemoresistance**

254 HIF-2α has been recognized as an important innate immunity regulator in the context of
255 tumours notably by controlling macrophage's recruitment (Imtiyaz *et al*, 2010). Moreover, we
256 recently reported that HIF-2α controls the expression of dihydropyrimidine dehydrogenase
257 (DPD) in hypoxia independently of its transcription factor activity. DPD expression in hypoxic
258 macrophages is responsible for a resistance to 5-fluorouracil in human colorectal cancers
259 (Malier *et al*, 2021). We demonstrated in the same study that rodent models are inadequate
260 to mimic that mechanism, due to an epigenetically negative control of the DPYD gene in
261 rodent macrophages contrary to what is found in humans. The downregulation of HIF-2α

262 expression under CSF-1R blockade offers a potential strategy to restore chemosensitivity in
263 that context. Indeed, edicotinib is able to downregulate the expression of DPD in hypoxic
264 macrophages (Figure 5A) leading to the complete abrogation of its enzymatic activity,
265 preventing the conversion of uracil into dihydrouracil (Figure 5B). We confirmed the inhibition
266 of the HIF-2α-dependent synthesis of DPD during the transition to hypoxia, which
267 necessitates the continuous destabilization of HIF-2α during the transition (Figure 5C). The
268 previous demonstration that ERK1/2 phosphorylation controls HIF-2α expression implies an
269 expected control of DPD expression in the same context as we confirmed (Figure 5D) as well
270 as the implication of the cellular cholesterol content in the hypoxic induced-DPD expression
271 in macrophages (Figure 5E). Consequently, the downregulation of DPD expression authorizes
272 the restoration of 5-FU sensitivity of HT-29 and RKO colorectal cancer cells in a co-culture
273 setting (Figure 5F). We previously demonstrated that DPD expression under the HIF-2α
274 expression is not related to mRNA modulation (Malier *et al*, 2021), to assure that this is still
275 the case in the tumour environment we demonstrated that edicotinib downregulates DPD
276 expression in hypoxic TAMs co-cultured with tumours (Figure 5G) without downregulation of
277 its mRNA as expected (Figure 5H). We previously demonstrated that macrophages represent
278 the main source of DPD expression in colorectal cancers (Malier *et al*, 2021). Nevertheless,
279 these macrophages are renewed by circulating monocytes and these hypoxic monocytes
280 (CD14+) express DPD contrary to other immune cells like hypoxic lymphocytes T (CD3+) or B
281 (CD19+) (Figure 5I & Supplemental Figure 5), representing another source of immune driven
282 chemoresistance toward 5-FU. Circulating monocytes are recruited to tumour sites thanks to
283 CCL2/CCL7 chemokines secretion from tumour macrophages (Qian *et al*, 2011; Sanford *et al*,
284 2013; Yang *et al*, 2020). Edicotinib is susceptible to interfere with this process. Indeed, the
285 gene ontology – biological process associated with myeloid leukocyte migration was related

286 to differentially downregulated genes by CSF-1R blockade (Figure 4A). We confirmed this
287 pattern through the action of CSF-1R targeting on the expression of *CCL2* and *CCL7* in
288 macrophages (Figure 5J). Similarly, CCL2 and CCL7 expressions are disrupted in hypoxic TAMs
289 exposed to edicotinib (Figure 5K). These results demonstrate the ability of CSF-1R targeting
290 to disrupt DPD expression in tumour-associated macrophages and prevent recruitment of
291 DPD expressing myeloid cells at the tumour site.

292 **Discussion**

293 Tumour associated macrophages represent an essential component of the tumour immune
294 microenvironment in a vast majority of cancers. Their implication in angiogenesis,
295 extracellular matrix remodelling, cancer cell proliferation, metastasis spreading and
296 resistance to treatment leads to the development of macrophage-centered therapeutic
297 strategies (Mantovani *et al*, 2022). The importance of the CSF-1/CSF-1R axis in macrophage
298 survival, differentiation and activation makes CSF-1R targeting a favoured approach to
299 reshape TAMs. Two strategies have been pursued to attain this goal: blocking the interaction
300 between the ligand (CSF-1, IL-34) with its receptor using specific anti-CSF-1R antibodies or
301 inhibiting the tyrosine kinase activity of CSF-1R using specific inhibitors. Various inhibitors
302 have been developed through the years, and despite high specificity against CSF-1R, these
303 molecules were unable to demonstrate a strong clinical effect when used as monotherapy
304 (El-Gamal *et al*, 2018; Mantovani *et al*, 2022). The unclear reasons for this lack of efficiency
305 drove us to design the current study to explore in detail the molecular consequences of CSF-
306 1R blockade using a selective CSF-1R kinase inhibitor (edicotinib or JNJ40346527) already
307 validated in humans (Genovese *et al*, 2015; von Tresckow *et al*, 2015).

308 We observe a clear metabolic shift in CSF-1R targeted macrophages mainly centered on
309 cholesterol and fatty acid metabolism. The link between CSF-1 and cholesterol metabolism
310 has been suggested in a previous study (Irvine *et al*, 2009). We confirm the ability of CSF-1 to
311 induce cholesterol synthesis and demonstrate that CSF-1R blockade is able to downregulate
312 *SREBF2* expression leading to the inhibition of the cholesterol synthesis but also its cellular
313 uptake. We observe that colorectal tumours favour *SREBF2* expression and as a consequence
314 drives the increase of cholesterol amount in human macrophages. Cholesterol efflux from
315 macrophages under the control of transporter proteins like ABCA1/ABCG1 has been
316 associated with tumour growth (Goossens *et al*, 2019). Tumour cells exposed to cholesterol
317 secreted by macrophages secrete hyaluronic acid that drives macrophage reprogramming
318 toward a M2 phenotype in mice (Goossens *et al*, 2019). Even if cholesterol transporters are
319 not repressed in macrophages targeted by edicotinib, the decreased total amount of cellular
320 cholesterol induced by edicotinib prevents the ability of macrophages to maintain their
321 secretion braking the back loop communication between tumour associated macrophages
322 and tumours.

323 As cholesterol is synthesized through the metabolic synthesis starting from acetyl-coA, which
324 is produced by the fatty acid β-oxidation pathway, we explored the fatty acid synthesis in
325 macrophages. We find that edicotinib is able to prevent the increase of fatty acid
326 accumulation driven by hypoxia in human macrophages (Figure 4E) preventing the
327 appearance of a immunosuppressive phenotype $CD206^{+}CD38^{+}$ induced by oleate
328 (Supplemental Figure 4).

329 CSF-1R blockade strategy is designed to happen in the low oxygen tumour environment. The
330 sensitivity of cholesterol synthesis and CSF-1 coupling in hypoxia is not known. A recent study

331 highlighted the importance of hypoxia in the induction of cholesterol synthesis in monocytes
332 but not in differentiated macrophages (Nakahara *et al*, 2023). The influence of CSF-1R
333 targeting on the hypoxic response reveals that *EPAS1* coding for HIF-2α is upregulated.
334 Associated with this observation, we note the inverse correlation between *EPAS1* mRNA and
335 HIF-2α protein that reveals the counter-regulation of *EPAS1* transcription by HIF-2α itself. A
336 similar observation has been suggested for HIF-1α, relying on miR-429 which expression is
337 promoted by HIF-1α (Bartoszewska *et al*, 2015). However, this negative feedback loop was
338 associated with the decrease of HIF-1α in chronic hypoxia. Our observation was done in
339 chronic hypoxia and no decrease of the protein HIF-2α was observed. This observation needs
340 to be further explored and the direct or indirect mechanism determined. Our observation of
341 the link between CSF-1R targeting and HIF-2α expression revealed the role of ERK1/2
342 activation in the stabilization of this hypoxia inducible factor in human macrophages. The
343 downregulation of HIF-2α opens a promising way to target the recently identified mechanism
344 leading to the chemoresistance to 5-FU driven by hypoxic macrophages in colorectal cancers
345 (Malier *et al*, 2021). We demonstrate, in this study, that targeting CSF-1R downregulates
346 ERK1/2 phosphorylation that in turn prevents HIF-2α expression in hypoxia preventing the
347 expression of DPD that can no longer degrade 5-fluorouracil. We further find that monocyte
348 recruitment driven by CCL2/CCL7 axis is also disrupted, preventing the contribution of other
349 myeloid DPD expressing cells to invade the tumour.

350 In this study, we have provided compelling evidences showing that CSF-1R blocking is an
351 effective strategy to prevent TAM commitment driven by cancer cells and to prevent
352 macrophage-induced resistance to chemotherapy. We have demonstrated the efficiency of a
353 CSF-1R kinase activity inhibitor to attain metabolic reprogramming of tumour associated

354 macrophages interfering with the cholesterol and fatty acid mediated cross-talk between

355 macrophage and cancer cells.

356 **Material and Methods**

357 **Resources**

Reagent or Resource	**Source**	**Reference/RRID**
Experimental Model		
HT-29	ATCC	HTB-38 / CVCL_0320
RKO	ATCC	CRL-2577 / CVCL_0504
THP-1	ATCC	TIB-202 / CVCL_0006
Antibodies		
Mouse anti β-Actin monoclonal antibody	Sigma	A2228 / AB_476697
Rabbit Anti-Lamin B1 polyclonal antibody	Cell Signaling Technology	13435/ AB_2737428
Rabbit anti-human CSF-1R polyclonal antibody	Cell Signaling Technology	3152 / AB_2085233
Rabbit anti-human Phospho-M-CSF Receptor (Tyr723) (49C10) monoclonal antibody	Cell Signaling Technology	3155 / AB_2085229
Mouse anti-DPD monoclonal antibody	Santa Cruz	Sc-271308 / AB_10610363
Rabbit anti-p44/42 MAPK (Erk1/2) (137F5) monoclonal antibody	Cell Signaling Technology	4695 / AB_390779
Rabbit anti- Phospho-p44/42 MAPK (Erk1/2) (Thr202/Tyr204) (D13.14.4E) monoclonal antibody	Cell Signaling Technology	4370 / AB_2315112
Mouse anti-HIF2α monoclonal antibody, unconjugated	Santa Cruz	Sc-46691 / AB_627523
Rabbit Anti-SREBP2 polyclonal antibody, Unconjugated	Abcam	Ab30682 / AB_779079
Anti -human CD14-FITC REAfinity	Miltenyi Biotec	REA599/ AB_2801871
Anti-human CD20-PE REAfinity	Miltenyi Biotec	REA780/ AB_2656072
Mouse Anti-human CD3-APC	BD Pharmingen	555342/ AB_398592
Mouse anti human-CD206	Santa Cruz	Sc-376232 / AB_10989352
STAT6 E10 mouse monoclonal	Santa Cruz	Sc-271213 / AB_10611300
pSTAT6 (pY641.18) mouse monoclonal	Santa Cruz	Sc-136019 / AB_2197371

TGM2 (CUB 7402) mouse monoclonal	Life Technologies	MA512739 / AB_10985077
CD14-FITC, human (REA599)	Miltenyi Biotec	130-110-518/ AB_2655049
CD206-PE, human	Miltenyi Biotec	130-095-220 / AB_10827704
RNA Extraction and RT-qPCR Kits		
iScript Ready-to-use cDNA supermix	Biorad	1708841
iTaq universal SYBR green supermix	Biorad	1725124
NucleoSpin RNA (250)	Macherey Nagel	740955.250
Media and reagents		
5-Fluorouracil (5-FU)	Roche	
β-mercaptoethanol	Sigma	M3148-100ML
Bovine Serum Albumin (BSA) solution 30%	Sigma	A9576-50ML
CD14 microbeads, human	Miltenyi Biotec	130-050-201
CD20 microbeads, human	Miltenyi Biotec	130-091-104
CD3 microbeads, human	Miltenyi Biotec	130-091-043
Human IL4, premium grade	Miltenyi Biotec	130-093-921
Human MCSF, premium grade	Miltenyi Biotec	130-096-489
Chloroform	Sigma	34854
DMSO for cell culture	Dutscher	702631
DPBS (1X) , no calcium, no magnesium	Life Technologies	14190169
Edicotinib	MedChemExpress	HY-109086
EDTA (0.5M), pH 8.0, RNase-free	Life Technologies	AM9260G
Fetal Bovine Serum (FBS), qualified, US	Life Technologies	26140079
HEPES (1M)	Life Technologies	15630056
Histopaque-1077	Sigma	10771-6X100ML
Human serum from male AB plasma (SAB)	Sigma	H4522-100ML
Methanol	Sigma	34860
RPMI 1640 medium, glutaMAX supplement	Life Technologies	61870044
Scyllo Inositol	Sigma	I8132
TrypLE Express Enzyme (1X), phenol red	Life Technologies	12605036
Tridecanoic Acid	Sigma	91988
Triton X-100	Fischer Scientific	85111
U0126	Sigma	662005
C75	Sigma	C5490
Oligonucleotides		
B2M forward	Eurogentec	5’ – GTGCTCGCGCTACTCTCTC – 3’
B2M reverse	Eurogentec	5’ – CGGATGGATGAAACCCAGACA – 3’
DPYD forward	Eurogentec	5’ - CGCAGGACCAGGGGTTTTAT - 3’
DPYD reverse	Eurogentec	5’ - TGGCAATGGAGAGTGACAGG - 3’
HPRT1 forward	Eurogentec	5’ – TGCTTTCCTTGGTCAGGCAG – 3’
HPRT1 reverse	Eurogentec	5’ – TTCGTGGGGTCCTTTTCACC – 3’
SREBF2 forward	Eurogentec	5’ – TGAGCCAGGAAGCCCTCTAT – 3’
SREBF2 reverse	Eurogentec	5’ – CAGAAGAATCCGTGAGCGGT – 3’
HMGCR forward	Eurogentec	5’ – GCTTTGCCCTTTTTCCTACTTTTG – 3’

HMGCR reverse	Eurogentec	5’ – ACCAACTCCAATCACAAGACATTC – 3’
DHCR7 forward	Eurogentec	5’ – GACCCTCATCAACCTGTCCTT – 3’
DHCR7 reverse	Eurogentec	5’ – GCAGATGTCAATGGTCTTCAGG – 3’
LDLR forward	Eurogentec	5’ – TACAAGTGCCAGTGTGAGGAA – 3’
LDLR reverse	Eurogentec	5’ – TTGGTGAAGAAGAGGTAGGCG – 3’
EPAS1 forward	Eurogentec	5‘ – GCAATCAGCTTCCTGCGAAC – 3’
EPAS1 reverse	Eurogentec	5’ – CGGCAATGAAACCCTCCAAG – 3’
FLT1 forward	Eurogentec	5’ – AAAGCCACCAACCAGAAGGG – 3’
FLT1 reverse	Eurogentec	5’ GCCACACAGGTGCATGTTAG – 3’
CCL2 forward	Eurogentec	5’ – AGCAGCAAGTGTCCCAAAGA – 3’
CCL2 reverse	Eurogentec	5’ – TTTGCTTGTCCAGGTGGTCC – 3’
CCL7 forward	Eurogentec	5’ – TGGAGAGCTACAGAAGGACCA – 3’
CCL7 reverse	Eurogentec	5’ – GGGTTTTCTTGTCCAGGTGCT – 3’
CSF-1 forward	Eurogentec	5’ – CAGCAAGAACTGCAACAACAGC – 3’
CSF-1 reverse	Eurogentec	5’ GGTCACTGCTAGGGATGGCT – 3’
CD206 forward	Eurogentec	5’ – CCATCGAGGAAGAGGTTCGG – 3’
CD206 reverse	Eurogentec	5’ – CCTGCAATCCCGGTTCTCAT – 3’
ON-TARGETplus Human SREBF2 (6721) siRNA - SMARTpool, 5 nmol	Dharmacon	L-009549-00-0005
ON-TARGETplus Non-Targeting pool, 5 nmol	Dharmacon	D-001810-10-05
ON-TARGETplus Human EPAS1 (2034) siRNA – SMARTpool, 5 nmol	Dharmacon	L-004814-00-0005
Others		
7-AAD staining solution	BD Biosciences	559925
Annexin V-FITC	Miltenyi Biotec	130-093-060
Cholesterol/Cholesteryl Ester Assay Kit - Quantification	Abcam	Ab65359
Cell Titer 96 Non-radioactive Cell Proliferation Assay (MTT)	Promega	G4000
LS columns	Miltenyi Biotec	130-042-401
Softwares		
Prism v7	GraphPad	
JMP v14	SAS	
Galileo	Integragen	

358

359 **Human samples**

360 Human blood samples from healthy de-identified donors were obtained from EFS (French

361 national blood service) as part of an authorized protocol (CODECOH DC-2018–3114). Donors

362 gave signed consent for use of their blood in this study. Tumorous and non tumourous tissues
363 were obtained from surgically resected colons at the university hospital of Grenoble Alpes
364 from patients included in the CRC-ORGA2 clinical trial (clinicaltrial.gov, NCT05038358).
365 Inclusion criteria comprise adult patients suffering from colorectal adenocarcinoma treated
366 by surgery without neoadjuvant chemotherapy (Table).

367 **Cell culture**

368 THP-1, RKO and HT-29, were purchased from ATCC. THP-1, HT-29 and RKO were maintained
369 in RPMI (Gibco) supplemented with 10% FBS (Gibco) at 37°C. All cells were routinely tested
370 for mycoplasma contamination using MycoAlert detection kit (Lonza).

371 **Human macrophage differentiation from monocytes**

372 Monocytes were isolated from leukoreduction system chambers of healthy EFS donors using
373 differential centrifugation (Histopaque 1077, Sigma) to obtain PBMCs. $CD14^+$ microbeads
374 (Miltenyi Biotec) were used to select monocytes according to the manufacturer's instructions.
375 Monocytes were plated in RPMI (Life Technologies) supplemented with 10% SAB (Sigma), 10
376 mM HEPES (Life Technologies), MEM Non-essential amino acids (Life Technologies) and 25
377 ng/mL M-CSF (Miltenyi Biotec). Differentiation was obtained after 6 days of culture. Hypoxic
378 cultures were performed in a hypoxic chamber authorizing an oxygen partial pressure control
379 (HypoxyLab, Oxford Optronix, UK). Hypoxia experiments were performed at 25 mmHg of
380 oxygen (~ 3%). $CD3^+$ T lymphocytes and $CD20^+$ B lymphocytes were sorted from PBMCs using
381 $CD3^+$ and $CD20^+$ microbeads (Miltenyi Biotec) according to the manufacturer's instructions.

382 **Preparation of tumour associated macrophages**

383 Tumorous and non-tumorous tissues obtained from colon of CRC patients. Tissues were kept
384 and transported in ice in RPMI medium supplemented with non-essential amino acids and
385 HEPES as well as antibiotics including penicillin-streptomycin and gentamicin and antifungal
386 amphotericin B. Tissues were minced in pieces of 2-4 mm^3 and deposited on cell culture
387 inserts (4 pieces by insert). These inserts were deposited in 6 well plates on 2 mL of RPMI +
388 10% human serum for 24 h. The resulting medium produced by tumorous and non-tumorous
389 tissues was then used to culture human monocyte derived macrophages for 48h to obtain
390 tumour-associated macrophages.

391 **Macrophage Conditioned Medium (MCM)**

392 THP1 macrophages were plated (12-wells plates) and differentiated at 500,000 cells with
393 50nM of PMA for 24 hours. THP1 macrophages were cultured at 3% oxygen and treated with
394 Edicotinib at 3µM or DMSO acting as a vehicle for 48 hours. Then 1µg/mL of 5-FU was used
395 to generate the 5FU Edicotinib MCM or 5FU Vehicle MCM during 24h. MCM was added for
396 48 hours to two distinct colon cancer cell lines, RKO and HT-29 cells, which were plated
397 previously at 100,000 cells per well (12-wells plates) for 24 hours. Then cancerous cells were
398 collected and counted and the percentage of growth inhibition was assessed for each
399 condition.

400 **RNAseq**

401 RNA extraction was performed using the NucleoSpin RNA kit components (Macherey Nagel)
402 according to the manufacturer's instructions. RNA sequencing was performed using an
403 Illumina HiSeq 4000 sequencer (Integragen). Gene expression quantification was performed
404 using the STAR software. STAR obtains the number of reads associated to each gene in the
405 Gencode v31 annotation (restricted to protein-coding genes, antisense and lincRNAs). Raw

406 counts for each sample were imported into R statistical software. Extracted count matrix was
407 normalized for library size and coding length of genes to compute FPKM expression levels.
408 The Bioconductor edgeR package was used to import raw counts into R statistical software.
409 Differential expression analysis was performed using the Bioconductor limma package and
410 the voom transformation. Gene ontology analysis was performed using the GONet software
411 (https://tools.dice-database.org/GOnet/). Gene list from the differential analysis was ordered
412 by decreasing log2 fold change. Gene set enrichment analysis (GSEA) was performed by
413 clusterProfiler::GSEA function using the fgsea algorithm.

414 **Lipidomics**

415 Human macrophages were metabolically quenched in dry ice – ethanol for one minute then
416 washed three times in cold PBS. Then total lipids were extracted in
417 chloroform/methanol/water (1:3:1, v/v/v) containing PC (C13:0/C13:0), 10 nmol and C21:0
418 (10 nmol) as internal standards for extraction) for 1 h at 4◦C, with periodic sonication. Then
419 polar and apolar metabolites were separated by phase partitioning by adding chloroform and
420 water to give the ratio of Chloroform/Methanol/Water, 2:1:0.8 (v/v/v). For lipid analysis, the
421 organic phase was dried under N2 gas and dissolved in 1-butanol to obtain1µl butanol/10^7
422 parasites.

423 *Total lipid analysis* – Total lipid was then added with 1 nmol pentadecanoic acid (C15:0) as
424 internal standard and derivatized to give fatty acid methyl ester (FAME) using
425 trimethylsulfonium hydroxide (TMSH, Machenery Nagel) for total glycerolipid content.
426 Resultant FAMEs were then analysed by GC-MS as previously described (Dubois *et al*, 2018).
427 All FAME were identified by comparison of retention time and mass spectra from GC-MS with

428 authentic chemical standards. The concentration of FAMEs was quantified after initial
429 normalization to different internal standards and finally to macrophage number.

430 **Immunoblotting**

431 Cells were lyzed in RIPA buffer supplemented with protease inhibitors (AEBSF 4 mM,
432 Pepstatine A 1 µM and Leupeptin 0.4 mM; Sigma Aldrich) and HIF-hydroxylase inhibitor
433 (DMOG 1 mM, Sigma Aldrich) for total lysate. Nuclear extracts have been obtained by
434 differential centrifugation between nuclei and cytoplasms after Triton-X100 (0.1% in Tris 20
435 mM and protease inhibitors) lysis of the cells. Nuclear pellets were secondarily lyzed in RIPA
436 Buffer and sonication. Proteins were quantified by BCA assay (ThermoFischer) and 15 µg of
437 total protein were run on SDS-PAGE gels. Proteins were transferred from SDS-PAGE gels to
438 PVDF membrane (Biorad), blocked with TBS-Tween supplemented with 5% milk, primary
439 antibodies were incubated at 1 µg/mL overnight 4°C. After washing with TBS, the membrane
440 was incubated with a horseradish peroxidase-conjugated secondary antibody (Jackson
441 Immunoresearch). Signal was detected by chemoluminescence (Fusion FX imaging system,
442 Vilber) after exposition to Clarity ECL substrate (Biorad).

443 **Flow cytometry**

444 Flow cytometry data was acquired on an Accuri C6 (BD) flow cytometer. Doublet cells were
445 gated out by comparing forward scatter signal height (FSC-H) and area (FSC-A). At least 10,000
446 events were collected in the analysis gate. Median fluorescence intensity (MFI) was
447 determined using Accuri C6 software (BD).

448 **DPD activity measurements**

449 These analyses were performed in the Pharmacology Laboratory of Institut Claudius-Regaud
450 (France) using an HPLC system composed of Alliance 2695 and diode array detector 2996
451 (Waters). Uracil (U), Dihydrouracil (UH2), Ammonium sulfate 99%, Acetonitrile (ACN) gradient
452 chromasolv for HPLC and 2-propanol were purchased from Sigma. Ethyl acetate Scharlau was
453 of HPLC grade and purchased from ICS (Lapeyrouse-Fossat, France). Water from Milli-Q
454 Advantage A10 and MultiScreen-HV 96-well Plates were used (Merck Millipore). Calibration
455 ranges were 3.125 – 200 ng/mL for U and 25 - 500 ng/mL for UH2 and 5-FU (5µg/mL) was
456 used as an internal standard.

457 **RNA isolation and qPCR analysis for gene expression**

458 Cells were directly lyzed and RNA was extracted using the NucleoSpin RNA kit components
459 (Macherey Nagel) according to the manufacturer's instructions. Reverse transcription was
460 performed using the iScript Ready-to-use cDNA supermix components (Biorad). qPCR was
461 then performed with the iTaq universal SYBR green supermix components (Biorad) on a CFX96
462 (Biorad). Quantification was performed using the ΔΔCt method using two different
463 housekeeping genes.

464 **Quantification of Cholesterol**

465 Macrophages were treated with 10 µM of Edicotinib or Simvastatin for 72 hours afterwhich
466 cells and supernatants were retrieved. Supernatants were stored at -80°C. Lipids were
467 extracted from cells using choloroform:isopropanol:NP-40 (7:11:0.1). Organic phase was
468 taken and air-dried at 50°C and stored at -80°C. The amount of cholesterol in cells and
469 supernatants was assessed using the cholesterol/cholesteryl ester assay quantification kit
470 (ab65359, abcam) according to the manufacturer's instructions.

471 **Silencing of EPAS1 and SREBF2**

472 Fully differentiated macrophages were transfected with siEPAS1 (L-004814-00-0005,
473 Dharmacon) or siSREBF2 (L-009549-00-0005, Dharmacon) at a final concentration of 5nmol/L
474 using Lipofectamine (RNAiMAx, Life Technologies).

475 **Statistical analysis**

476 Statistics were performed using Graph Pad Prism 7 (Graph Pad Software Inc). When two
477 groups were compared, we used a paired or unpaired two-tailed student's t test when
478 appropriate. When more than two groups were compared, we used a one-way ANOVA
479 analysis with Sidak's multiple comparison test on paired data when appropriate. The
480 likelihood of data according to a null-hypothesis (p-value) are presented within the figures.
481 The number of independent experiments used to generate data are represented on each
482 figures.

483 **Data Availability**

484 The data generated and analyzed will be made from the corresponding author on reasonable
485 request.

486 **Acknowledgments**

487 KG has been supported by the ITN (International Training Network) Phys2Biomed project,
488 which was funded from the European Union's Horizon 2020 research and innovation
489 programme under the Marie Skłodowska-Curie grant agreement No 812772 and is supported
490 by the ERiCAN program of Fondation MSD-Avenir (Reference DS-2018-0015). CGP is
491 supported by the Innovative Research Initiative (IRGA 2022) of the university Grenoble Alpes.
492 MM is supported by the APMC Fondation (Agir pour les Maladies Chroniques). This work is

supported by the Ligue Régionale contre le Cancer. We thank Malika Yakoubi for her technical support on DPD chromatographic activity measurment. We thank Dr Lemoigne, Dr Federspiel and Dr Plasse from the University Hospital of Grenoble-Alpes for kindly providing clinical grade 5-Fluorouracil.

Contributions

KG, CGP, MM, CH, RG, AM performed experiments and analysed the data. AM supervised the data analysis. FT performed chromatography measurements. YB, CB performed the lipidomics analysis. GR, EG recruited patients. MHL performed the pathological analysis. AM wrote the original draft and all authors were involved in manuscript editing. Funding acquisition and supervision of the study was performed by AM.

References

Bartoszewska S, Rochan K, Piotrowski A, Kamysz W, Ochocka RJ, Collawn JF & Bartoszewski R (2015) The hypoxia-inducible miR-429 regulates hypoxia-inducible factor-1α expression in human endothelial cells through a negative feedback loop. *FASEB J* 29: 1467–1479

Cannarile MA, Weisser M, Jacob W, Jegg A-M, Ries CH & Rüttinger D (2017) Colony-stimulating factor 1 receptor (CSF-1R) inhibitors in cancer therapy. *J Immunother Cancer* 5: 53

Conrad PW, Freeman TL, Beitner-Johnson D & Millhorn DE (1999) EPAS1 trans-Activation during Hypoxia Requires p42/p44 MAPK*. *J Biol Chem* 274: 33709–33713

Cortese N, Carriero R, Laghi L, Mantovani A & Marchesi F (2020) Prognostic significance of tumor-associated macrophages: past, present and future. *Semin Immunol* 48: 101408

DeNardo DG & Ruffell B (2019) Macrophages as regulators of tumour immunity and immunotherapy. *Nat Rev Immunol* 19: 369–382

Dotson RJ, Smith CR, Bueche K, Angles G & Pias SC (2017) Influence of Cholesterol on the Oxygen Permeability of Membranes: Insight from Atomistic Simulations. *Biophys J* 112: 2336–2347

Dubois D, Fernandes S, Amiar S, Dass S, Katris NJ, Botté CY & Yamaryo-Botté Y (2018) Toxoplasma gondii acetyl-CoA synthetase is involved in fatty acid elongation (of long fatty acid chains) during tachyzoite life stages. *J Lipid Res* 59: 994–1004

El-Gamal MI, Al-Ameen SK, Al-Koumi DM, Hamad MG, Jalal NA & Oh C-H (2018) Recent Advances of Colony-Stimulating Factor-1 Receptor (CSF-1R) Kinase and Its Inhibitors. *J Med Chem* 61: 5450–5466

523 Engblom C, Pfirschke C & Pittet MJ (2016) The role of myeloid cells in cancer therapies. *Nat Rev*
524 *Cancer* 16: 447–462

525 Genovese MC, Hsia E, Belkowski SM, Chien C, Masterson T, Thurmond RL, Manthey CL, Yan X
526 (David), Ge T, Franks C, *et al* (2015) Results from a Phase IIA Parallel Group Study of JNJ-
527 40346527, an Oral CSF-1R Inhibitor, in Patients with Active Rheumatoid Arthritis despite
528 Disease-modifying Antirheumatic Drug Therapy. *J Rheumatol* 42: 1752–1760

529 Goossens P, Rodriguez-Vita J, Etzerodt A, Masse M, Rastoin O, Gouirand V, Ulas T, Papantonopoulou
530 O, Van Eck M, Auphan-Anezin N, *et al* (2019) Membrane Cholesterol Efflux Drives Tumor-
531 Associated Macrophage Reprogramming and Tumor Progression. *Cell Metab* 29: 1376–
532 1389.e4

533 Horton JD, Shimomura I, Brown MS, Hammer RE, Goldstein JL & Shimano H (1998) Activation of
534 cholesterol synthesis in preference to fatty acid synthesis in liver and adipose tissue of
535 transgenic mice overproducing sterol regulatory element-binding protein-2. *J Clin Invest* 101:
536 2331–2339

537 Imtiyaz HZ, Williams EP, Hickey MM, Patel SA, Durham AC, Yuan L-J, Hammond R, Gimotty PA, Keith
538 B & Simon MC (2010) Hypoxia-inducible factor 2α regulates macrophage function in mouse
539 models of acute and tumor inflammation. *J Clin Invest* 120: 2699–2714

540 Irvine KM, Andrews MR, Fernandez-Rojo MA, Schroder K, Burns CJ, Su S, Wilks AF, Parton RG, Hume
541 DA & Sweet MJ (2009) Colony-stimulating factor-1 (CSF-1) delivers a proatherogenic signal to
542 human macrophages. *J Leukoc Biol* 85: 278–288

543 Lachmann A, Xu H, Krishnan J, Berger SI, Mazloom AR & Ma'ayan A (2010) ChEA: transcription factor
544 regulation inferred from integrating genome-wide ChIP-X experiments. *Bioinformatics* 26:
545 2438–2444

546 Malier M, Gharzeddine K, Laverriere M-H, Marsili S, Thomas F, Decaens T, Roth G & Millet A (2021)
547 Hypoxia Drives Dihydropyrimidine Dehydrogenase Expression in Macrophages and Confers
548 Chemoresistance in Colorectal Cancer. *Cancer Res* 81: 5963–5976

549 Mantovani A, Allavena P, Marchesi F & Garlanda C (2022) Macrophages as tools and targets in
550 cancer therapy. *Nat Rev Drug Discov*: 1–22

551 McGettrick AF & O'Neill LAJ (2020) The Role of HIF in Immunity and Inflammation. *Cell Metab* 32:
552 524–536

553 Nakahara R, Aki S, Sugaya M, Hirose H, Kato M, Maeda K, Sakamoto DM, Kojima Y, Nishida M, Ando
554 R, *et al* (2023) Hypoxia activates SREBP2 through Golgi disassembly in bone marrow-derived
555 monocytes for enhanced tumor growth. *EMBO J* n/a: e114032

556 Nes WD (2011) Biosynthesis of Cholesterol and Other Sterols. *Chem Rev* 111: 6423–6451

557 O'Brien SA, Orf J, Skrzypczynska KM, Tan H, Kim J, DeVoss J, Belmontes B & Egen JG (2021) Activity of
558 tumor-associated macrophage depletion by CSF-1R blockade is highly dependent on the
559 tumor model and timing of treatment. *Cancer Immunol Immunother* 70: 2401–2410

560 Pradel LP, Ooi C-H, Romagnoli S, Cannarile MA, Sade H, Rüttinger D & Ries CH (2016) Macrophage
561 Susceptibility to Emactuzumab (RG7155) Treatment. *Mol Cancer Ther* 15: 3077–3086

562 Pyonteck SM, Akkari L, Schuhmacher AJ, Bowman RL, Sevenich L, Quail DF, Olson OC, Quick ML, Huse
563 JT, Teijeiro V, *et al* (2013) CSF-1R inhibition alters macrophage polarization and blocks glioma
564 progression. *Nat Med* 19: 1264–1272

565 Qian B-Z, Li J, Zhang H, Kitamura T, Zhang J, Campion LR, Kaiser EA, Snyder LA & Pollard JW (2011)
566 CCL2 recruits inflammatory monocytes to facilitate breast-tumour metastasis. *Nature* 475:
567 222–225

568 Ries CH, Cannarile MA, Hoves S, Benz J, Wartha K, Runza V, Rey-Giraud F, Pradel LP, Feuerhake F,
569 Klaman I, *et al* (2014) Targeting Tumor-Associated Macrophages with Anti-CSF-1R Antibody
570 Reveals a Strategy for Cancer Therapy. *Cancer Cell* 25: 846–859

571 Sanford DE, Belt BA, Panni RZ, Mayer A, Deshpande AD, Carpenter D, Mitchem JB, Plambeck-Suess
572 SM, Worley LA, Goetz BD, *et al* (2013) Inflammatory Monocyte Mobilization Decreases
573 Patient Survival in Pancreatic Cancer: A Role for Targeting the CCL2/CCR2 Axis. *Clin Cancer*
574 *Res* 19: 3404–3415

575 Stanley ER & Chitu V (2014) CSF-1 Receptor Signaling in Myeloid Cells. *Cold Spring Harb Perspect Biol*
576 6: a021857

577 The ENCODE (ENCyclopedia Of DNA Elements) Project (2004) *Science*

578 von Tresckow B, Morschhauser F, Ribrag V, Topp MS, Chien C, Seetharam S, Aquino R, Kotoulek S, de
579 Boer CJ & Engert A (2015) An Open-Label, Multicenter, Phase I/II Study of JNJ-40346527, a
580 CSF-1R Inhibitor, in Patients with Relapsed or Refractory Hodgkin Lymphoma. *Clin Cancer*
581 *Res* 21: 1843–1850

582 Wilson WR & Hay MP (2011) Targeting hypoxia in cancer therapy. *Nat Rev Cancer* 11: 393–410

583 Wu H, Han Y, Rodriguez Sillke Y, Deng H, Siddiqui S, Treese C, Schmidt F, Friedrich M, Keye J, Wan J,
584 *et al* (2019) Lipid droplet-dependent fatty acid metabolism controls the immune suppressive
585 phenotype of tumor-associated macrophages. *EMBO Mol Med* 11: e10698

586 Yang H, Zhang Q, Xu M, Wang L, Chen X, Feng Y, Li Y, Zhang X, Cui W & Jia X (2020) CCL2-CCR2 axis
587 recruits tumor associated macrophages to induce immune evasion through PD-1 signaling in
588 esophageal carcinogenesis. *Mol Cancer* 19: 1–14

589

590

591

592

593

594

595

596

597

598

599

600

601

602

603

604

605

606

607

608 Figures Legends

609 Figure 1. **Complete CSF-1R inhibition is associated with a profound phenotypic change**.

610 (A) Immunoblot of phosphorylated CSF-1R at site Tyrosine 723, CSF-1R total protein and β-
611 actin (upper panel). Quantification of the level of phosphorylation normalised to β-actin from
612 three independent experiments.

613 (B) Flow cytometry analysis of 7-AAD+ cells treated for 48h. Each condition has its own vehicle
614 control (DMSO) at the same concentration than edicotinib (Ed) (n=3).

615 (C) MTT assay on cells exposed to Edicotinib for 48h (n=3).

616 (D) Volcano-plot analysis of differentially expressed genes between edicotinib vs vehicle
617 (n=4).

618 (E) GO (Gene Ontology)-term analysis of biological processes associated with downregulated
619 genes under edicotinib exposure. Number of genes associated with each GO-terms are
620 indicated.

621 Figure 2. **CSF-1/CSF-1R controls cholesterol synthesis in human macrophages associated**
622 **with tumours**

623 (A) Gene expression of cholesterol synthesis enzymes in human macrophages treated by
624 edicotinib (in red) compared to controls (vehicle in black) (n=4). Gene expression levels are
625 expressed in FPKM=Fragments Per Kilobase Million.

626 (B) The cholesterol synthesis pathway with intermediate products. Enzymes which present a
627 downregulation with a fold change >2 are represented in red.

628 (C) Expression of *HMGCR* and *DHRC7* genes after 6h stimulation by CSF-1 50 ng/mL on
629 previously starved human macrophages determinded by RT-qCPR (n=3).

630 (D) Representation of SREBP2 target genes based on ChIP analysis (ENCODE study).

631 (E) Expression of *SREBF2*, *HMGCR*, *DHCR7* and *LDLR* genes in RNAi treated macrophages
632 against *SREBF2* determined by RT-qPCR (n=5).

633 (F) Expression of *SREBF2* gene after 6h stimulation by CSF-1 50 ng/mL on previously starved
634 human macrophages determinded by RT-qCPR (n=3).

635 (G) Gene expression of *SREBF2* in human macrophages treated by edicotinib (n=4). Gene
636 expression levels are expressed in FPKM=Fragments Per Kilobase Million.

637 (H) Representative immunoblot of nuclear SREBP2 in human macrophages treated with
638 edicotinib compared to controls (Upper panel) using Lamin B as a control loading.
639 Quantification of SREBP2 normalized to the control loading is represented in the lower panel
640 (n=4).

641 (I) Gene expression of *LDLR* in human macrophages treated by edicotinib (n=4). Gene
642 expression levels are expressed in FPKM=Fragments Per Kilobase Million.

643 (J) Quantification of intracellular cholesterol in macrophages treated by edicotinib or
644 simvastatin and in RNAi against SREBF2 treated macrophages compared to vehicle (DMSO) or
645 RNAi control respectively (n=3). The amount of decrease is represented in % compared to the
646 appropriate control.

647 (K) Macroscopic view of a colon adenocarcinoma and HES staining of tumorous and non-
648 tumorous tissues used in a co-culture with human macrophages.

649 (L) Expression of *SREBF2*, *HMGCR*, *DHCR7* and *LDLR* genes in hypoxic macrophages cultured
650 with non tumorous and tumorous tissues determined by RT-qPCR (n=5). Tumour associated
651 macrophages were also treated by edicotinib. Relative expression compared to control
652 macrophages in normoxia.

653 (M) ELISA quantification of IL-34 and CSF-1 secreted by tumorous and non-tumorous tissues
654 (n=4).

655 (N) Flow cytometry quantification of membrane CSF-1R expression on macrophages treated
656 by edicotinib compared to controls (DMSO) (n=3).

657 (O) Gene expression of *CSF-1* in human macrophages treated by edicotinib (n=4). Gene
658 expression levels are expressed in FPKM=Fragments Per Kilobase Million.

659 (P) Expression of *CSF-1* gene in hypoxic macrophages cultured with non tumorous and
660 tumorous tissues determined by RT-qPCR (n=4). Tumour associated macrophages were also
661 treated by edicotinib. Relative expression compared to control macrophages in normoxia.

662 Figure 3. **CSF-1R targeting downregulates HIF2α expression in hypoxia through ERK1/2**
663 **phosphorylation inhibition.**

664 (A) Hierarchical clustering (Ward methodology) of hypoxic responsive genes ($\log_2$ FC <-1 and
665 $\log_2$ FC >-1 and q-value < 0.05) for normoxic and hypoxic macrophages exposed to edicotinib
666 and vehicle (DMSO).

667 (B) Gene expression of *LDHA, NDRG1, P4HA1* and *SLC2A1* genes in normoxic and hypoxic
668 human macrophages treated by edicotinib or vehicle (n=4). Gene expression levels are
669 expressed in FPKM=Fragments Per Kilobase Million. Normoxia is in blue and hypoxia is in red.

670 (C) Gene expression of *EPAS1* gene in normoxic and hypoxic human macrophages treated by
671 edicotinib or vehicle (n=4). Gene expression levels are expressed in FPKM=Fragments Per
672 Kilobase Million. Normoxia is in blue and hypoxia is in red.

673 (D) Immunoblot of HIF-2α in normoxic and hypoxic macrophages (Representative of five
674 independent experiments).

675 (E) Gene expression of *FLT1* gene in normoxic and hypoxic human macrophages treated by
676 edicotinib or vehicle (n=4). Gene expression levels are expressed in FPKM=Fragments Per
677 Kilobase Million. Normoxia is in blue and hypoxia is in red.

678 (F) Immunoblot of HIF-2α in normoxic and hypoxic macrophages treated by vehicle or
679 edicotinib with a representative experiment (left panel) and quantification of the expression
680 of HIF-2α compared to βactin (right panel) (n=4).

681 (G) Gene Set Enrichment Analysis of the Gene Ontology – Biological Process ERK1 and ERK2
682 cascade for hypoxic macrophages treated by edicotinib.

683 (H) Immunoblot of phosphorylated ERK1/2, total ERK1/2 and βactin in edicotinib treated
684 macrophages (Representative of three independent experiments).

685 (I) Immunoblot of HIF-2α in normoxic and hypoxic macrophages treated by vehicle, edicotinib
686 or U0126 (10µM) with a representative experiment (left panel) and quantification of the
687 expression of HIF-2α compared to βactin (right panel) (n=3).

688 (J) Immunoblot of HIF-2α in normoxic and hypoxic macrophages treated by siRNA against
689 SREBF2 or using siRNA scrambled with a representative experiment (left panel) and
690 quantification of the expression of HIF-2α compared to βactin (right panel) (n=3).

691 Figure 4. **Fatty acid synthesis in hypoxia is reversed by CSF-1R targeting.**

692 (A) GO (Gene Ontology)-term analysis of biological processes associated with downregulated
693 genes under edicotinib exposure in hypoxia. Number of genes associated with each GO-terms
694 are indicated.

695 (B) Heat map of cholesterol synthesis genes associated with *SREBF1*, *FASN* and *SREBF2* for
696 hypoxic macrophages treated by edicotinib compared to vehicle.

697 (C) GO (Gene Ontology)-term analysis of biological processes associated with genes identified
698 in cluster 4 of figure 3A. Number of genes associated with each GO-terms are indicated.

699 (D) Fatty acid synthesis pathway involving the fatty acid synthetase (FASN).

700 (E) Quantification by GS-MS of palmitic acid (C16:0), stearic acid (C18:0), palmitoleic acid
701 (C16:1 cis) and oleic acid (C18:1 cis) in macrophages in normoxia, in hypoxia and in hypoxia
702 treated by edicotinib (n=4).

703 (F) Quantification by flow cytometry of CD206 membrane expression in co-cultured
704 macrophages with RKO cells and IL-4 (25 ng/mL) for 48 h with vehicle (DMSO) or edicotinib
705 (n=3). Representative panel on the left and quantification on the right.

706 (G) Expression of *CD206 (MRC1)* gene in hypoxic macrophages stimulated by IL-4 for 4 hours
707 and a specific inhibitor of FASN (C75 50 µM) determined by RT-qPCR (n=3).

708 Figure 5. **CSF-1R targeting downregulates the expression of dihydropyrimidine**
709 **dehydrogenase in tumour associated macrophages**

710 (A) Immunoblot of DPD in normoxic and hypoxic macrophages treated by vehicle (DMSO) and
711 edicotinib with a representative experiment (upper panel) and quantification of the
712 expression of HIF-2α compared to βactin (lower panel) (n=4).

713 (B) Quantification of the reductive activity of DPD through the conversion of uracil (U) to
714 dihydrouracil (UH_2) (n=4).

715 (C) Immunoblot of HIF-2α, DPD and βactin for macrophages treated by edicotinib for 48h then
716 submitted to 6h hypoxia with or without maintaining the CSF-1R blockade (+6h condition).
717 Representative of three independent experiments.

718 (D) Immunoblot of DPD and βactin for macrophages treated by edicotinib or U0126 for 48h
719 then submitted to 6h hypoxia with edicotinib or U0126. A representative experiment is shown
720 in the upper panel and the quantification compared to βactin appears in the lower panel
721 (n=3).

722 (E) Immunoblot of DPD and βactin for macrophages treated by siRNA against SREBF2 or SiRNA
723 scrambled for 48h then submitted to 6h hypoxia. A representative experiment is shown in the
724 upper panel and the quantification compared to βactin appears in the lower panel (n=3).

725 (F) Co-culture between colorectal cancers cells (HT-29, RKO) with human THP1-macrophages.
726 Inhibition of the proliferation rate of cancer cells treated by 5-FU conditioned by macrophages
727 MCM (5-FU) or added to macrophage conditioned medium MCM + 5-FU. The conditioning is
728 performed with edicotinib (5µM) or vehicle (DMSO) (n=3). MCM= Macrophage Conditioned
729 Medium.

730 (G) Immunoblot of DPD and β-actin in hypoxic tumour associated macrophages treated by
731 edicotinib or vehicle (DMSO) (representative of three experiments).

732 (H) Expression of *DPYD* gene in hypoxic macrophages cultured with non-tumorous and
733 tumorous tissues determined by RT-qPCR. Tumour associated macrophages were also treated
734 by edicotinib (n=5). Relative expression compared to control macrophages in normoxia.

735 (I) Immunoblot of DPD and β-actin in CD14+ monocytes, CD3+ T lymphocytes and CD20+ B
736 lymphocytes (representative of three independent healthy donors).

737 (J) Gene expression of *CCL2* and *CCL7* in hypoxic human macrophages treated by edicotinib
738 (n=4). Gene expression levels are expressed in FPKM=Fragments Per Kilobase Million.

739 (K) Expression of *CCL2* and *CCL7* genes in hypoxic macrophages cultured with non-tumorous
740 and tumorous tissues determined by RT-qPCR (n=5). Tumour associated macrophages were
741 also treated by edicotinib. Relative expression compared to control macrophages in
742 normoxia.

743 (L) Schematics of CSF-1 controlled tumour associated macrophages involvement in tumour
744 growth and consequences of CSF-1R targeting. Figure created using Biorender
745 (biorender.com)

746

747 **Supplementary Figure Legends**

748 Supplemental Figure 1

749 Flow cytometry analysis of Annexin-V+ cells treated for 48h. Each condition has its own
750 vehicle control (DMSO) at the same concentration than edicotinib (Ed) (n=3).

751 Supplemental Figure 2

752 (A) Gene expression of *ABCA1* and *ABCG1* genes in human macrophages treated by edicotinib
753 (n=4). Gene expression levels are expressed in FPKM=Fragments Per Kilobase Million.

754 (B) Quantification of extracellular cholesterol secreted by macrophages treated by edicotinib
755 or simvastatin compared to vehicle (DMSO) (n=3). The amount of decrease is represented in
756 % compared to the control.

757 Supplemental Figure 3

758 (A) Flow cytometry analysis of Annexin-V+ cells treated for 48h in hypoxia. Each condition has
759 its own vehicle control (DMSO) at the same concentration than edicotinib (Ed) (n=3).

760 (B) Immunoblot of HIF-2α in macrophages in hypoxia (6h) treated by siRNA against SREBF2 or
761 using siRNA scrambled compared to normoxia (representative of three independent
762 experiments, left panel). Expression of *FLT1* gene after 6h in hypoxia in the same macrophages
763 than in the left panel determined by RT-qCPR (right panel) (n=3).

764 (C) Expression of *HMGCR*, *DHCR7* and *LDLR* genes in hypoxic macrophages treated by
765 edicotinib or U0126 (10 µM) or vehicle determined by RT-qPCR (n=3). Relative expression
766 compared to control macrophages in normoxia.

767 Supplemental Figure 4

768 (A) Immunoblot of CD206 in hypoxic macrophages co-cultured with tumours exposed to
769 edicotinib vs vehicle (DMSO) for 24h. Representative of three independent experiments.

770 (B) Gene expression of *CD206* and *CD38* genes in human macrophages treated by edicotinib
771 in hypoxia. Gene expression levels are expressed in FPKM=Fragments Per Kilobase Million.

772 Supplemental Figure 5

773 Flow cytometry analysis of sorted Monocytes, T lymphocytes and B lymphocytes using CD14,
774 CD3 and CD20 expression respectively. Representative of three independent experiments on
775 healthy donors.

Figure 1

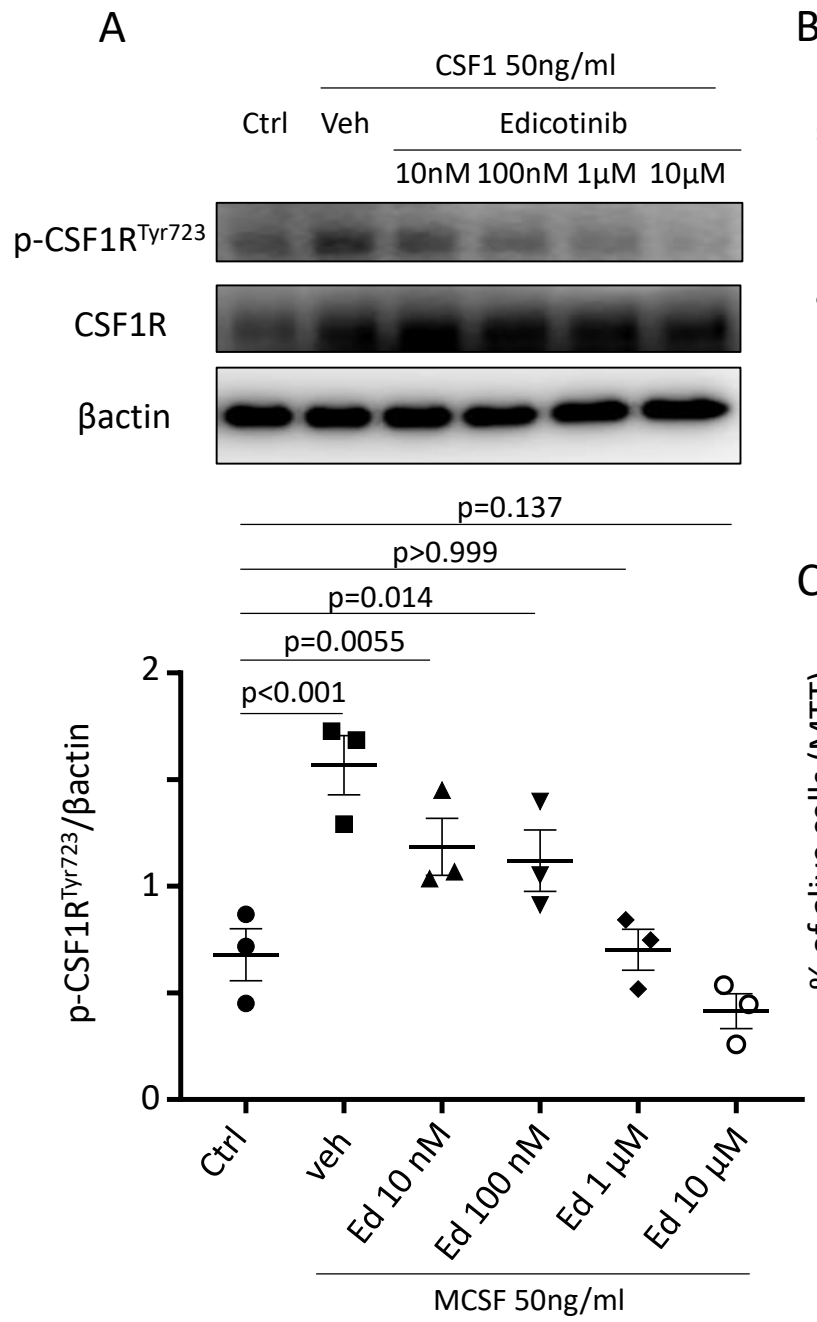
A
CSF1 50ng/ml
Ctrl
Veh
Edicotinib
10nM 100nM 1µM 10µM
p-CSF1R Tyr723
CSF1R
βactin
p=0.137
p>0.999
p=0.014
p=0.0055
p<0.001
p-CSF1R Tyr723/βactin
0
1
2
Ctrl
veh
Ed 10 nM
Ed 100 nM
Ed 1 µM
Ed 10 µM
MCSF 50ng/ml

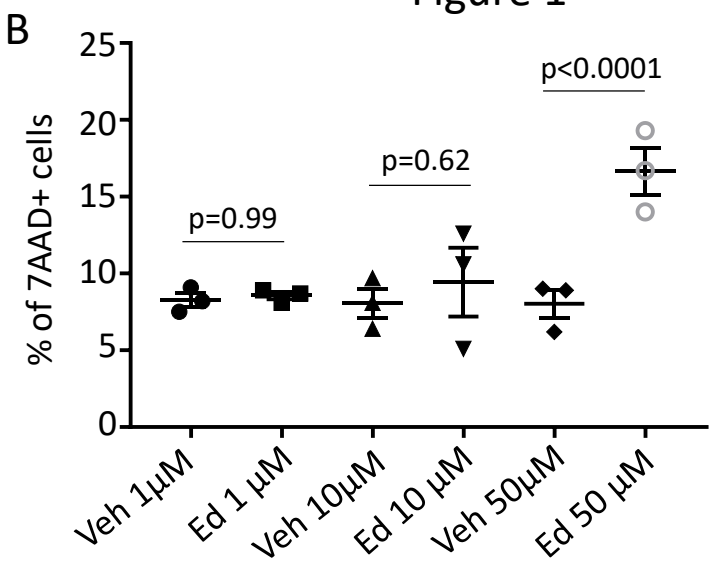
B
% of 7AAD+ cells
0
5
10
15
20
25
p=0.99
p=0.62
p<0.0001
Veh 1µM
Ed 1 µM
Veh 10µM
Ed 10 µM
Veh 50µM
Ed 50 µM

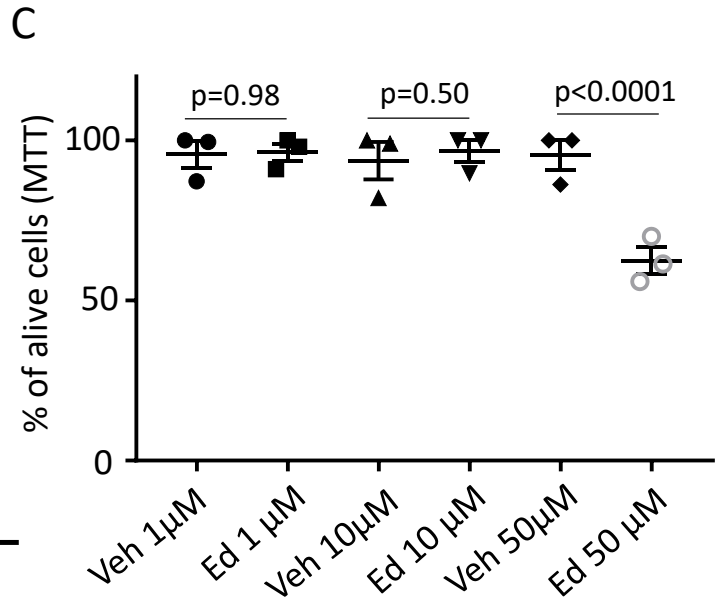
C
% of alive cells (MTT)
0
50
100
p=0.98
p=0.50
p<0.0001
Veh 1µM
Ed 1 µM
Veh 10µM
Ed 10 µM
Veh 50µM
Ed 50 µM

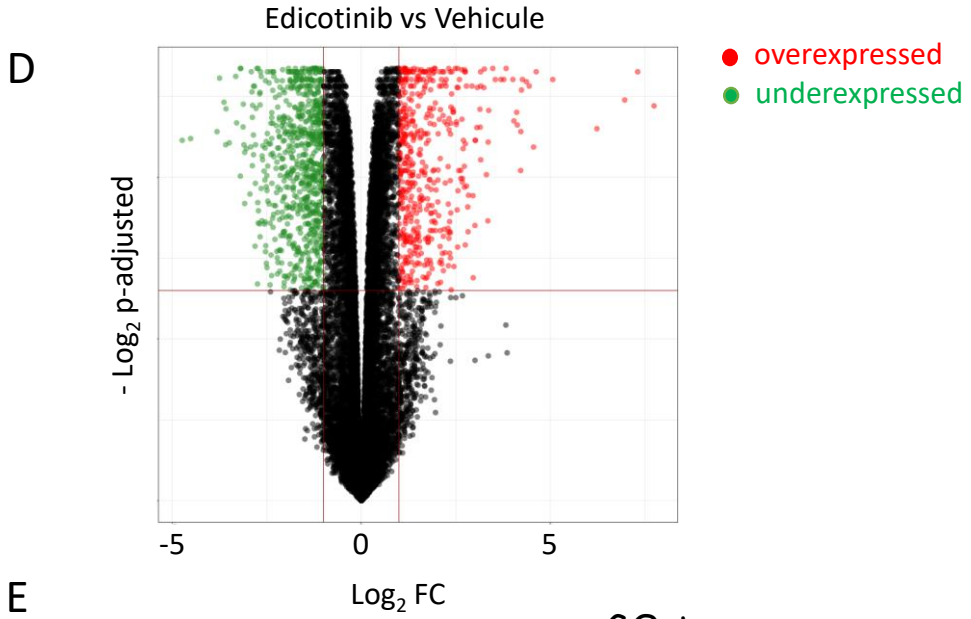
D
Edicotinib vs Vehicule
overexpressed
underexpressed
- Log2 p-adjusted
Log2 FC
-5
0
5

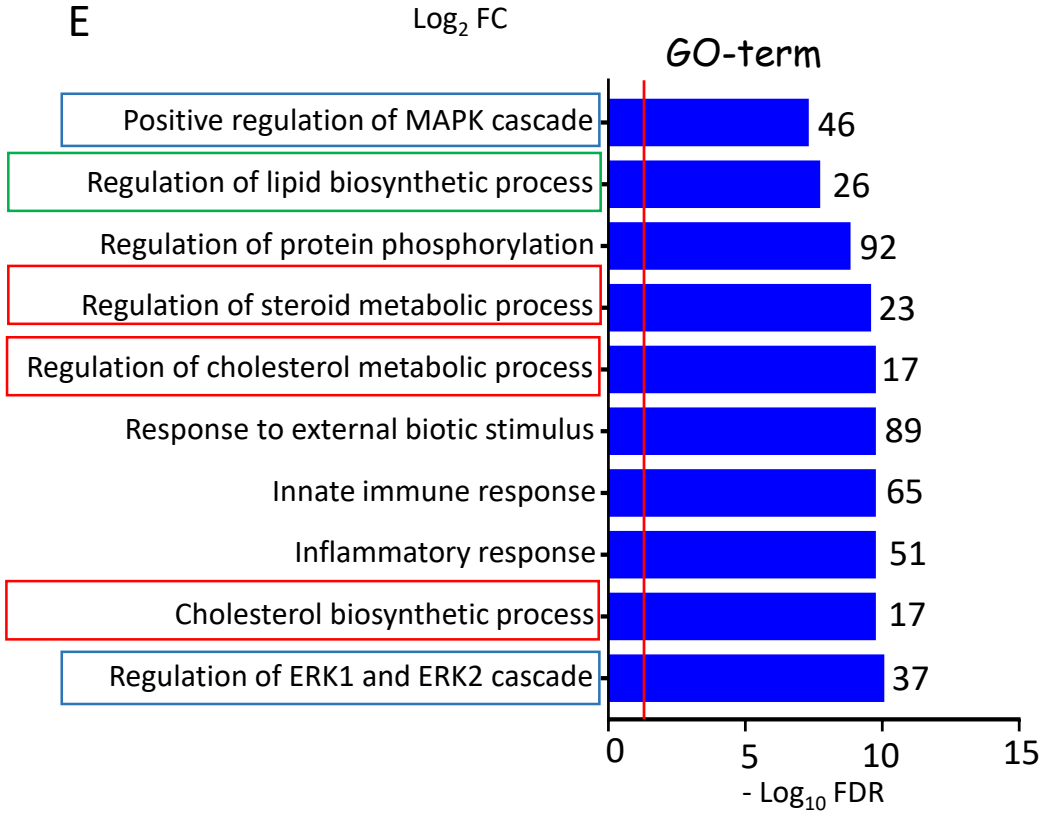
E
GO-term
Positive regulation of MAPK cascade 46
Regulation of lipid biosynthetic process 26
Regulation of protein phosphorylation 92
Regulation of steroid metabolic process 23
Regulation of cholesterol metabolic process 17
Response to external biotic stimulus 89
Innate immune response 65
Inflammatory response 51
Cholesterol biosynthetic process 17
Regulation of ERK1 and ERK2 cascade 37
0
5
10
15
- Log10 FDR

Supplemental Figure 1

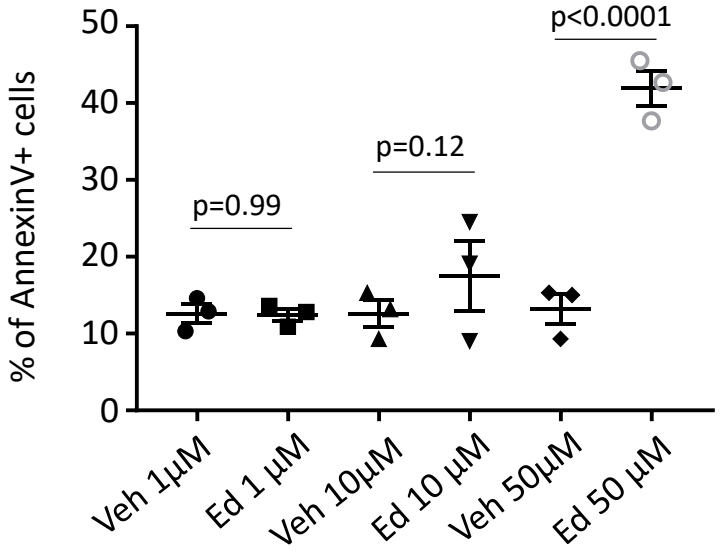

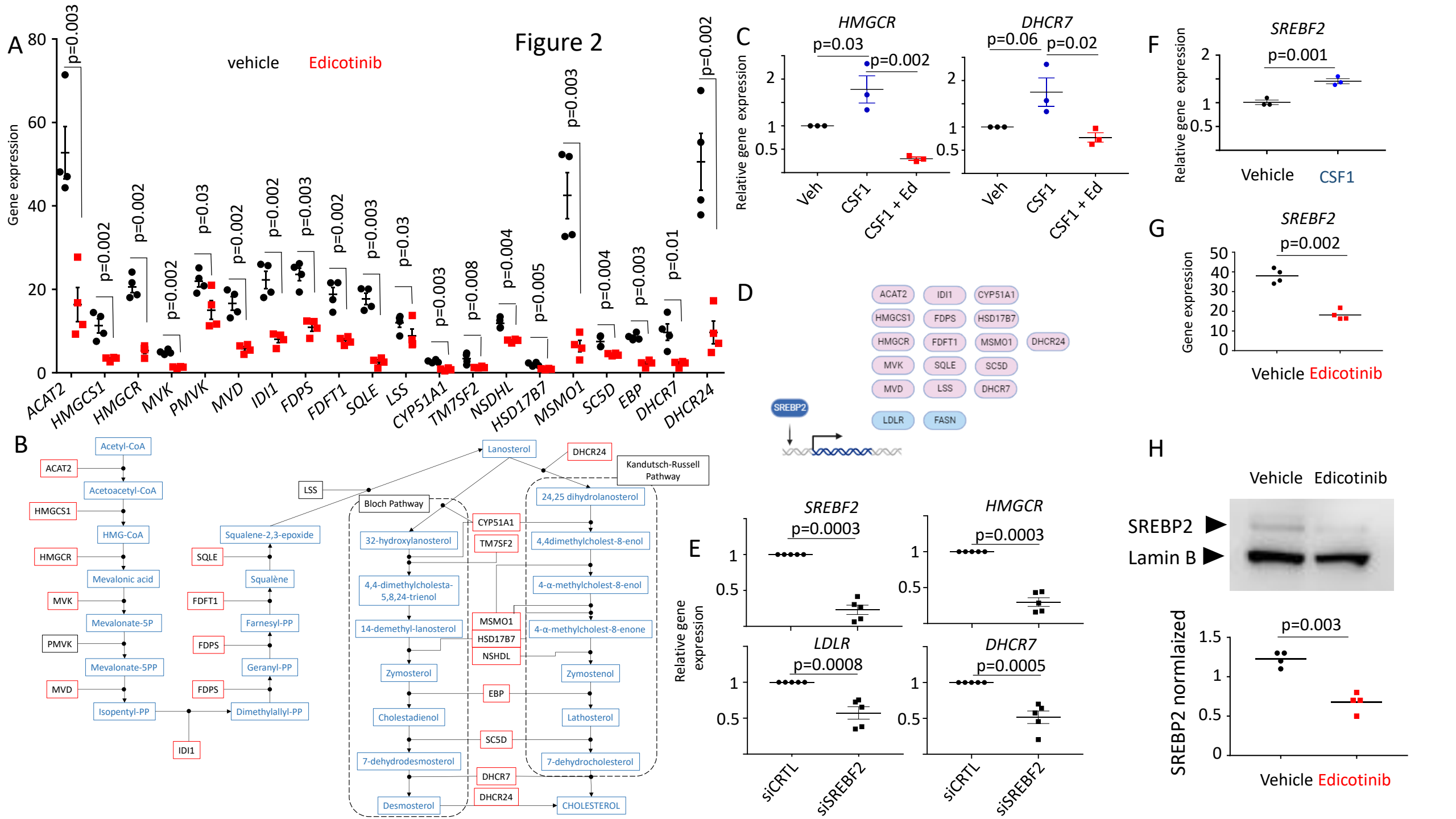
Figure 2
A
vehicle
Edicotinib
Gene expression
ACAT2
HMGCS1
HMGCR
MVK
PMVK
MVD
IDI1
FDPS
FDFT1
SQLE
LSS
CYP51A1
TM7SF2
NSDHL
HSD17B7
MSMO1
SC5D
EBP
DHCR7
DHCR24
B
Acetyl-CoA
Acetoacetyl-CoA
HMG-CoA
Mevalonic acid
Mevalonate-5P
Mevalonate-5PP
Isopentyl-PP
Dimethylallyl-PP
Geranyl-PP
Farnesyl-PP
Squalène
Squalene-2,3-epoxide
Lanosterol
Bloch Pathway
Kandutsch-Russell Pathway
32-hydroxylanosterol
4,4-dimethylcholesta-5,8,24-trienol
14-demethyl-lanosterol
Zymosterol
Cholestadienol
7-dehydrodesmosterol
Desmosterol
24,25 dihydrolanosterol
4,4dimethylcholest-8-enol
4-α-methylcholest-8-enol
4-α-methylcholest-8-enone
Zymostenol
Lathosterol
7-dehydrocholesterol
CHOLESTEROL
C
HMGCR
DHCR7
Relative gene expression
Veh
CSF1
CSF1 + Ed
D
SREBP2
E
SREBF2
HMGCR
LDLR
DHCR7
siCRTL
siSREBF2
F
SREBF2
Vehicle
CSF1
G
SREBF2
Gene expression
Vehicle
Edicotinib
H
Vehicle
Edicotinib
SREBP2
Lamin B
SREBP2 normlaized

Figure 2

I

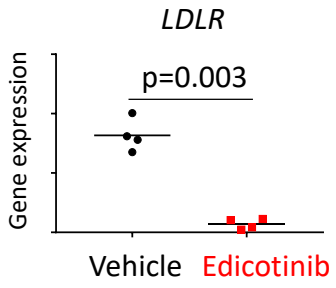

J

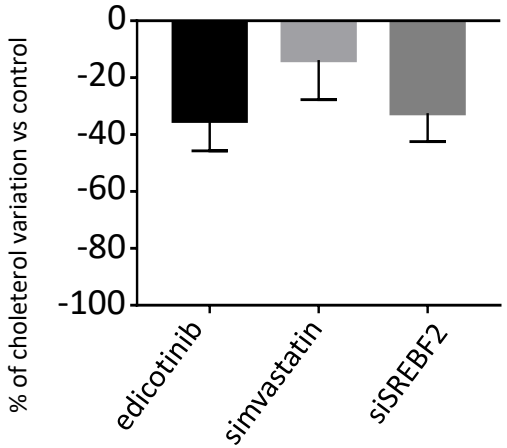

K

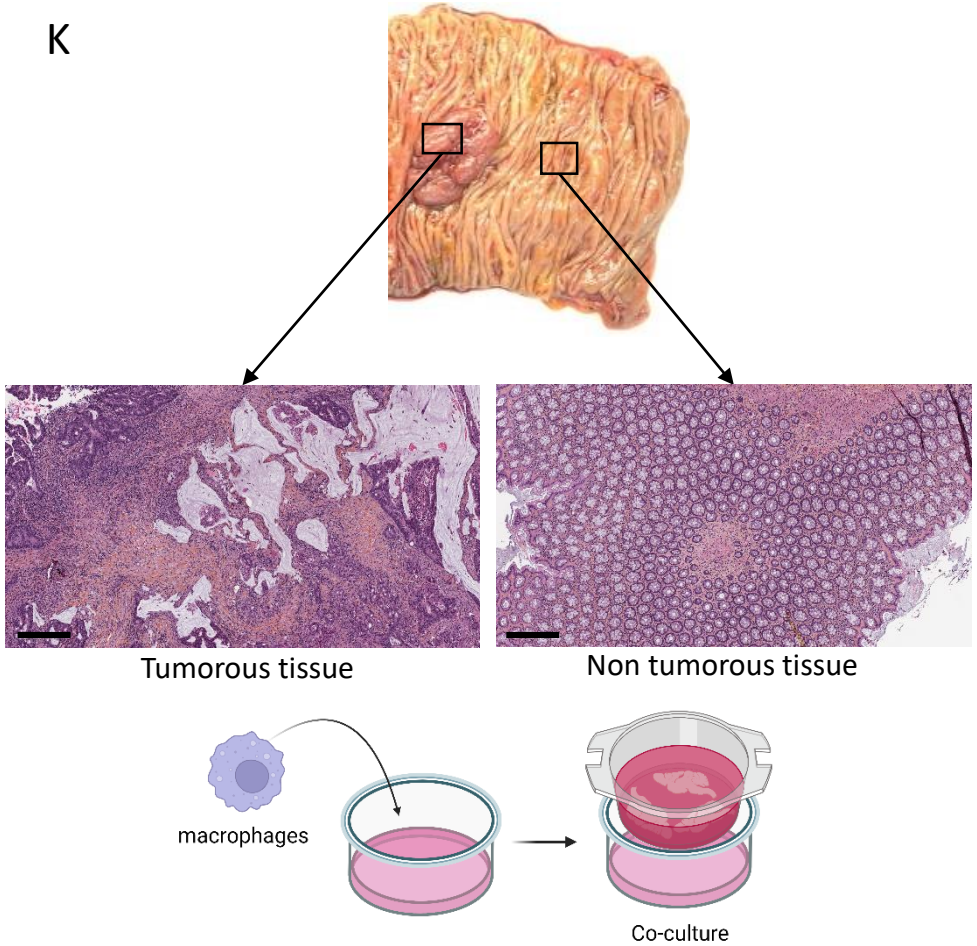

L

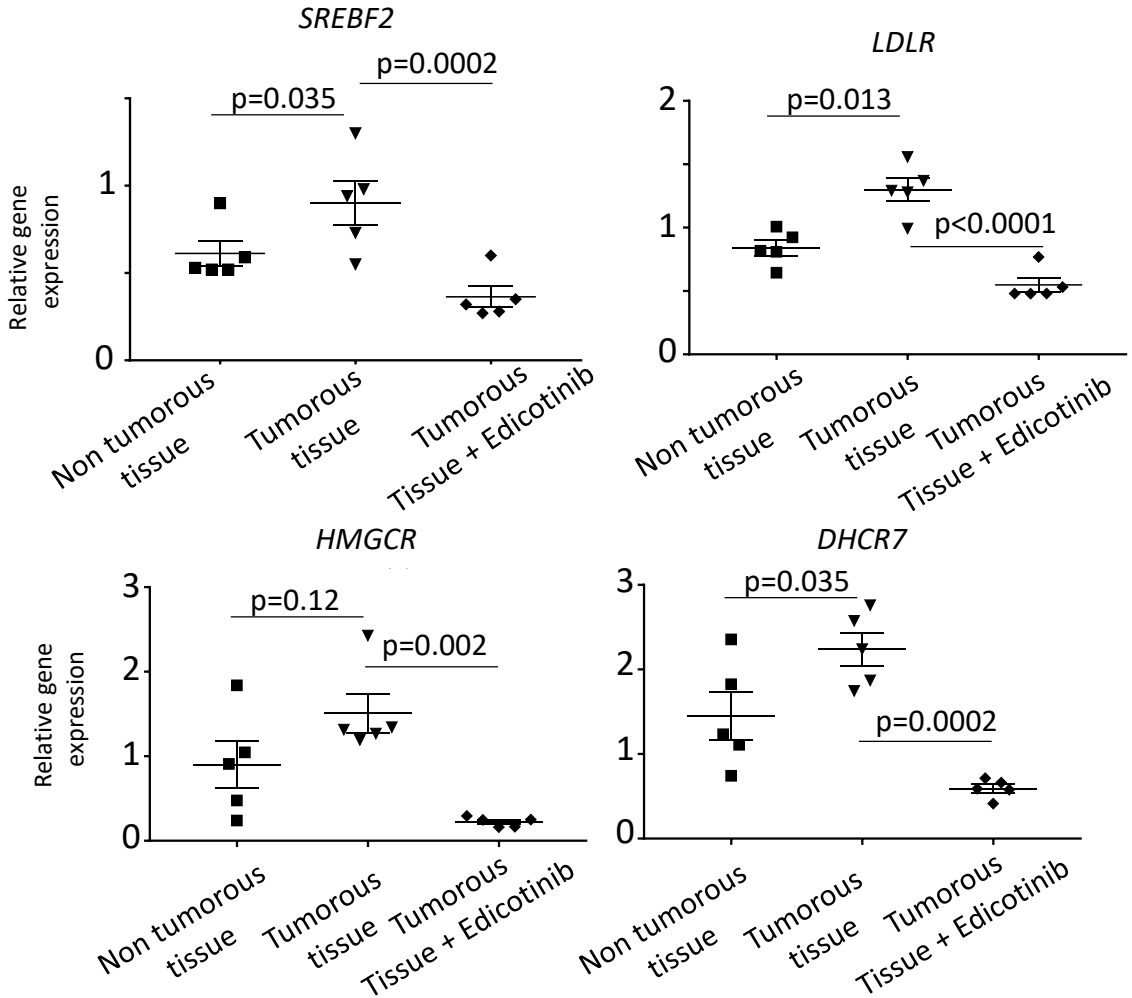

Figure 2

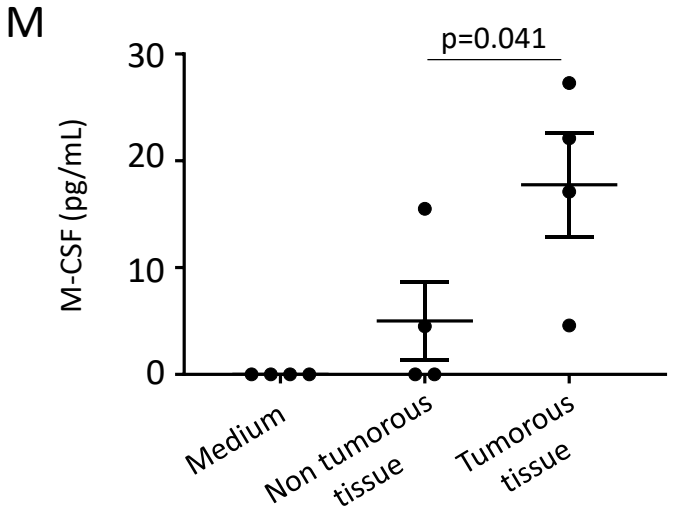
M
p=0.041
M-CSF (pg/mL)
30
20
10
0
Medium
Non tumorous tissue
Tumorous tissue

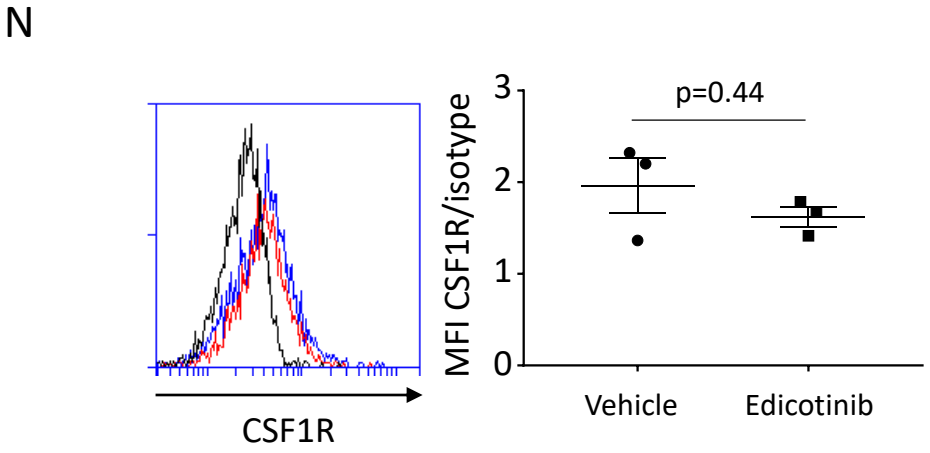
N
CSF1R
p=0.44
MFI CSF1R/isotype
3
2
1
0
Vehicle
Edicotinib

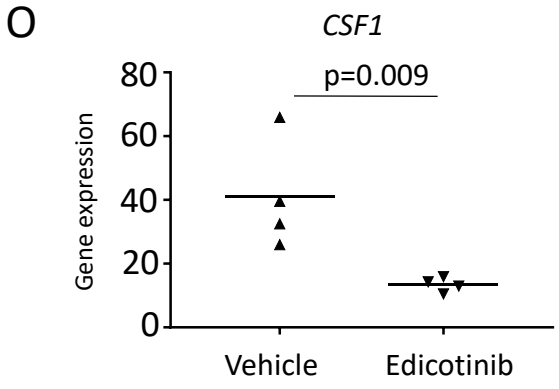
O
CSF1
p=0.009
Gene expression
80
60
40
20
0
Vehicle
Edicotinib

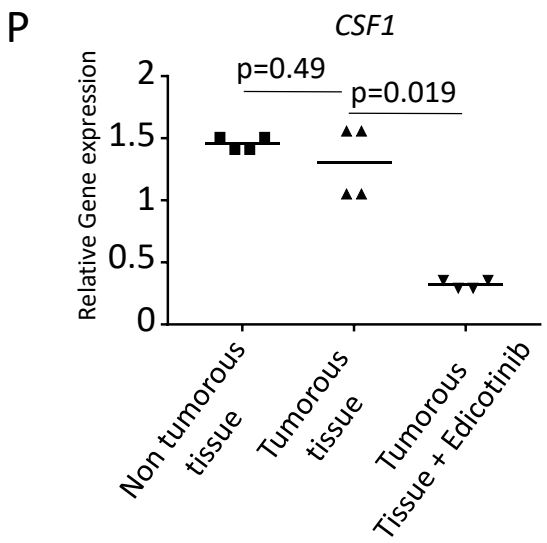
P
CSF1
p=0.49
p=0.019
Relative Gene expression
2
1.5
1
0.5
0
Non tumorous tissue
Tumorous tissue
Tumorous Tissue + Edicotinib

Supplemental Figure 2

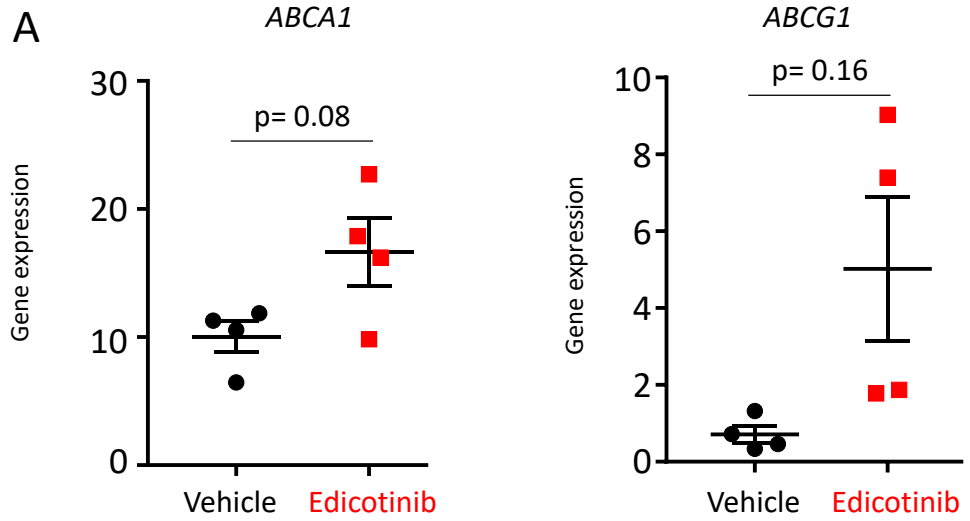

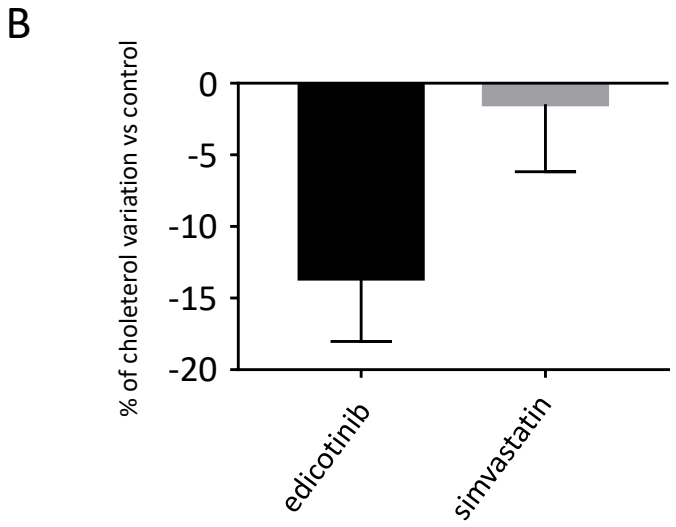

Figure 3

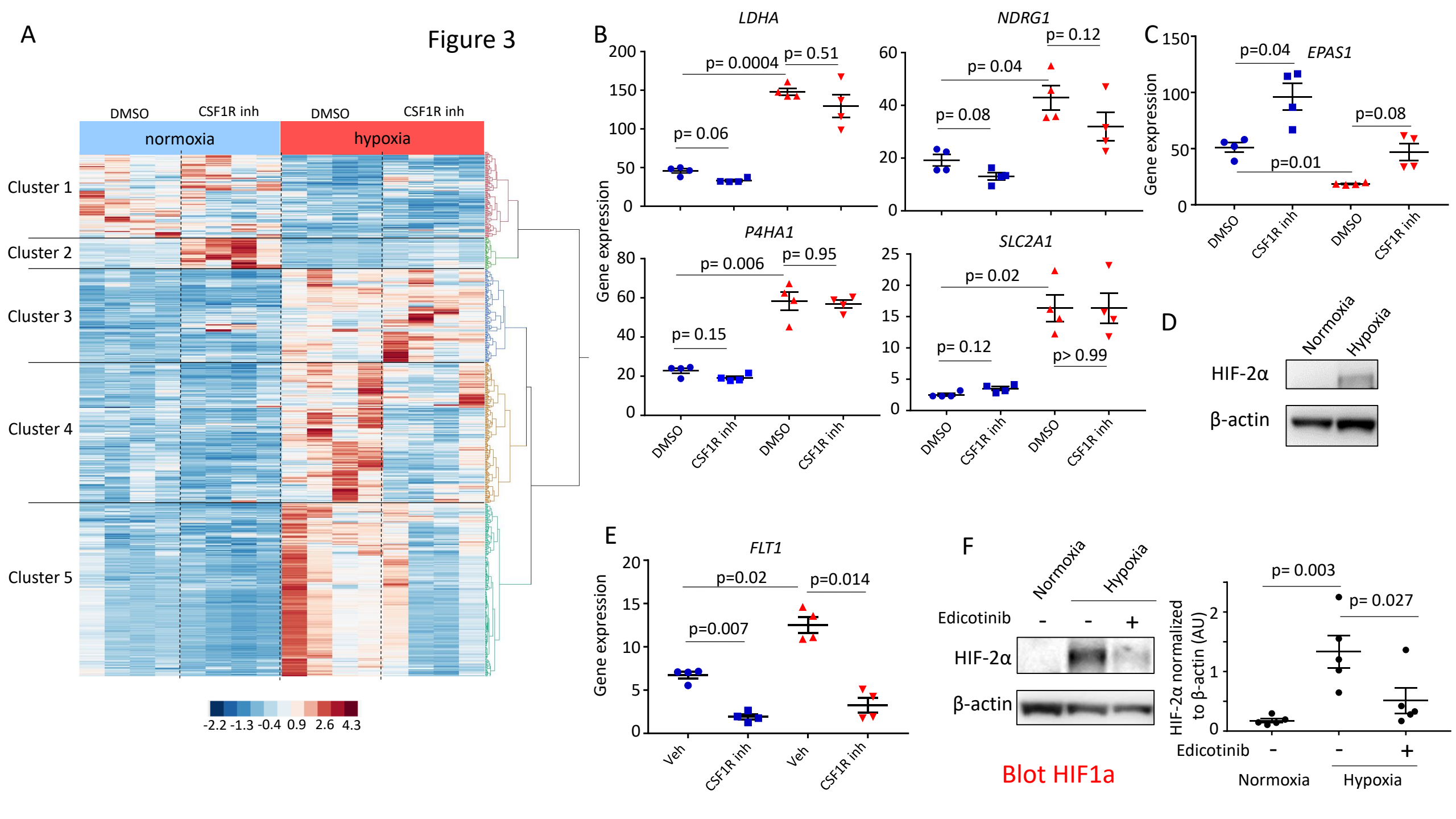
A
DMSO
CSF1R inh
DMSO
CSF1R inh
normoxia
hypoxia
Cluster 1
Cluster 2
Cluster 3
Cluster 4
Cluster 5
-2.2 -1.3 -0.4 0.9 2.6 4.3
B
LDHA
p= 0.0004
p= 0.51
p= 0.06
NDRG1
p= 0.12
p= 0.04
p= 0.08
P4HA1
p= 0.006
p= 0.95
p= 0.15
SLC2A1
p= 0.02
p= 0.12
p> 0.99
Gene expression
DMSO
CSF1R inh
DMSO
CSF1R inh
C
EPAS1
p=0.04
p=0.08
p=0.01
Gene expression
DMSO
CSF1R inh
DMSO
CSF1R inh
D
Normoxia
Hypoxia
HIF-2α
β-actin
E
FLT1
p=0.02
p=0.014
p=0.007
Gene expression
Veh
CSF1R inh
Veh
CSF1R inh
F
Normoxia
Hypoxia
Edicotinib
-
-
+
HIF-2α
β-actin
Blot HIF1a
p= 0.003
p= 0.027
HIF-2α normalized to β-actin (AU)
Edicotinib
-
-
+
Normoxia
Hypoxia

G

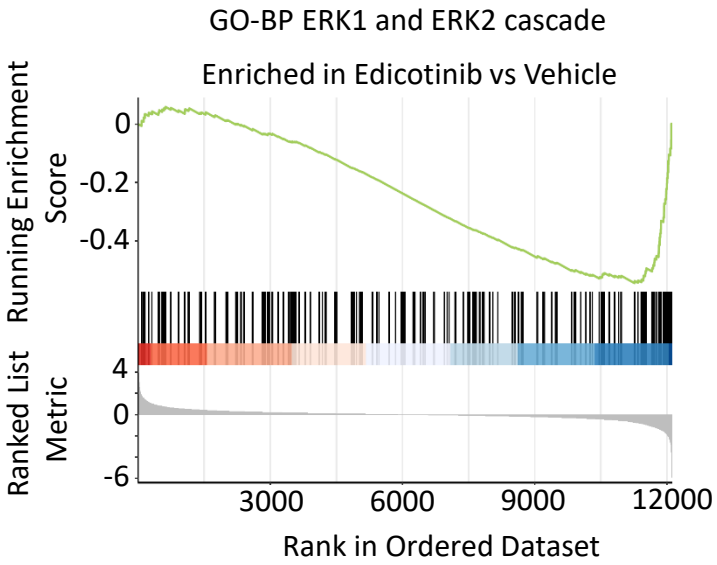

H

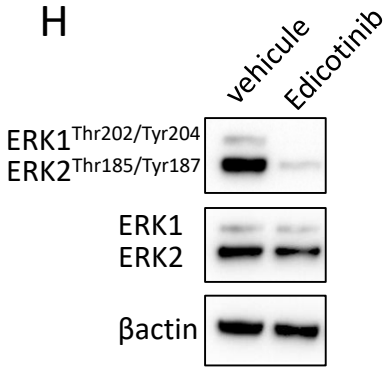

Figure 3

I

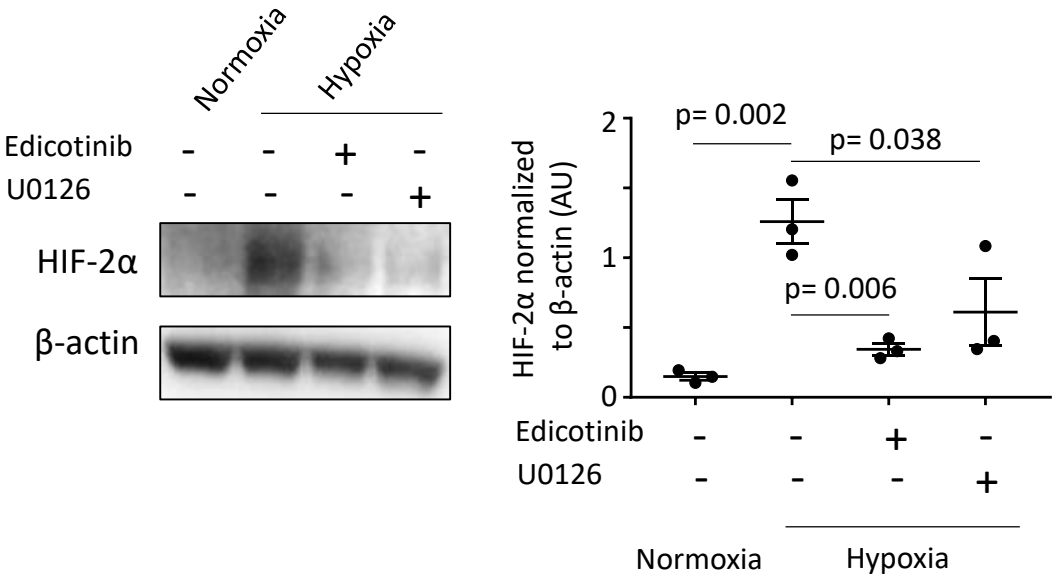

J

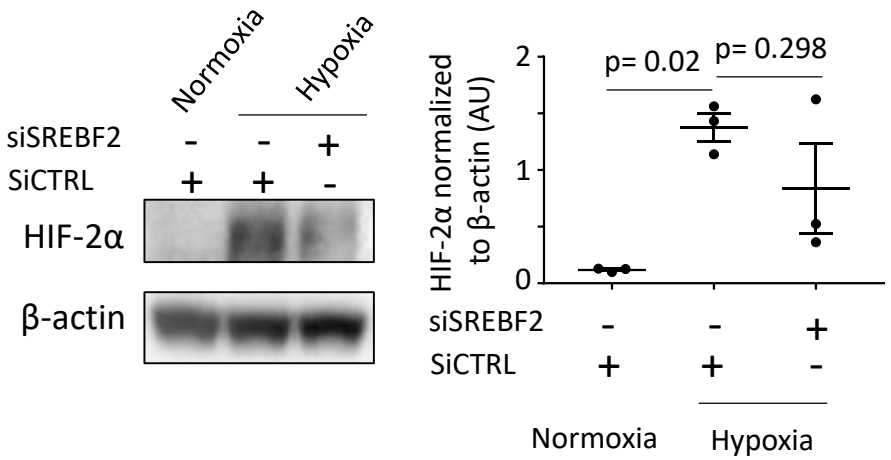

Supplemental Figure 3

A

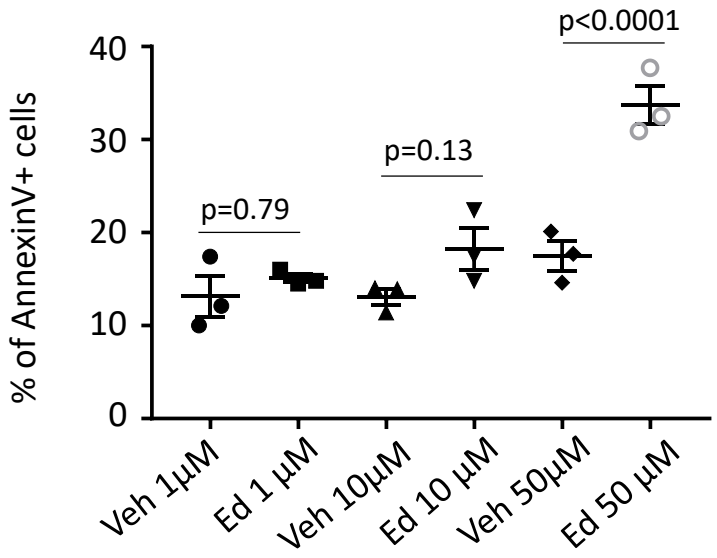

B

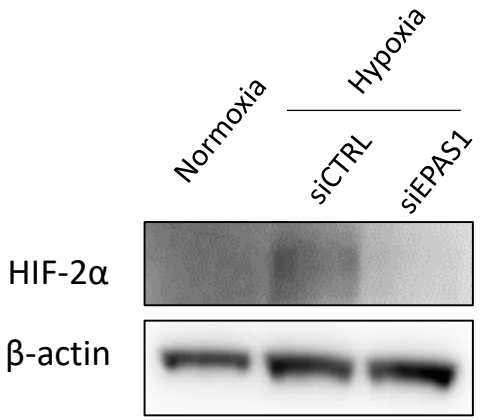

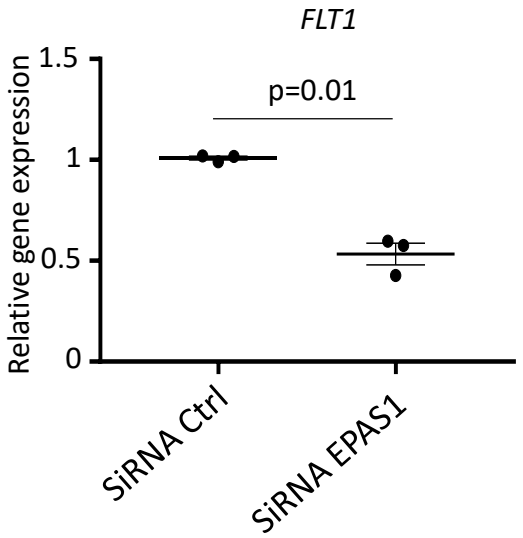

C

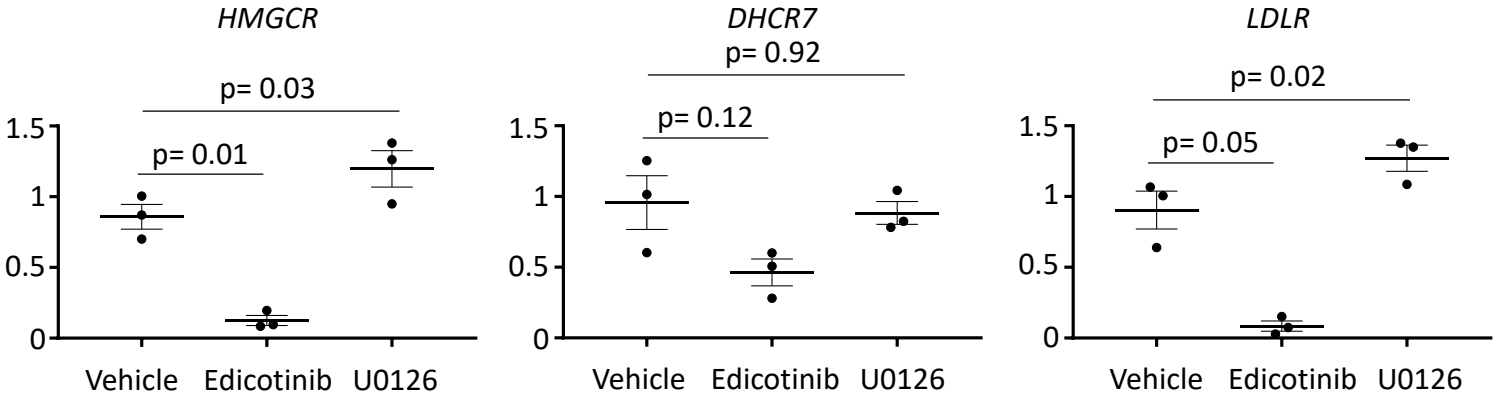

Figure 4

A

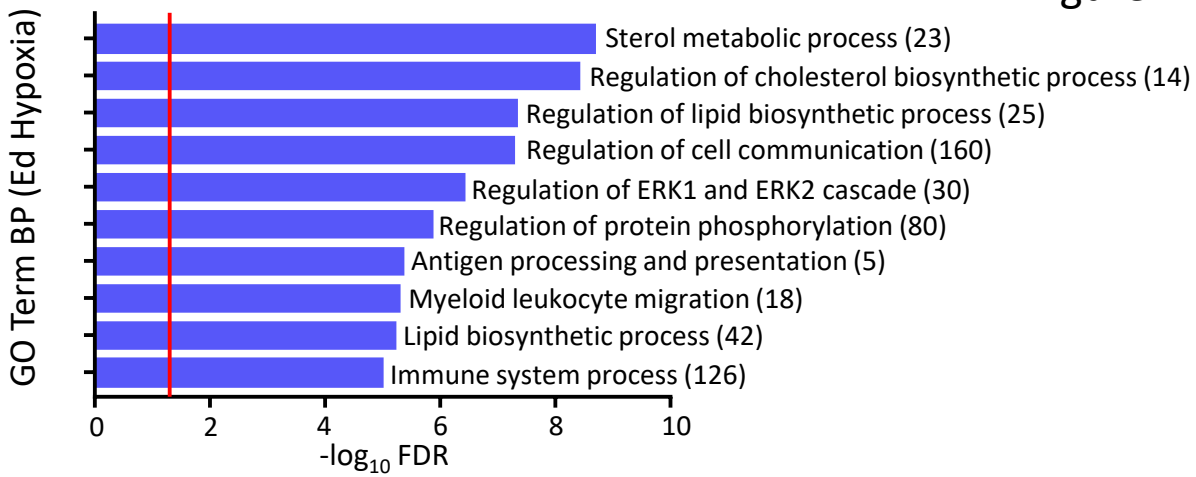

C

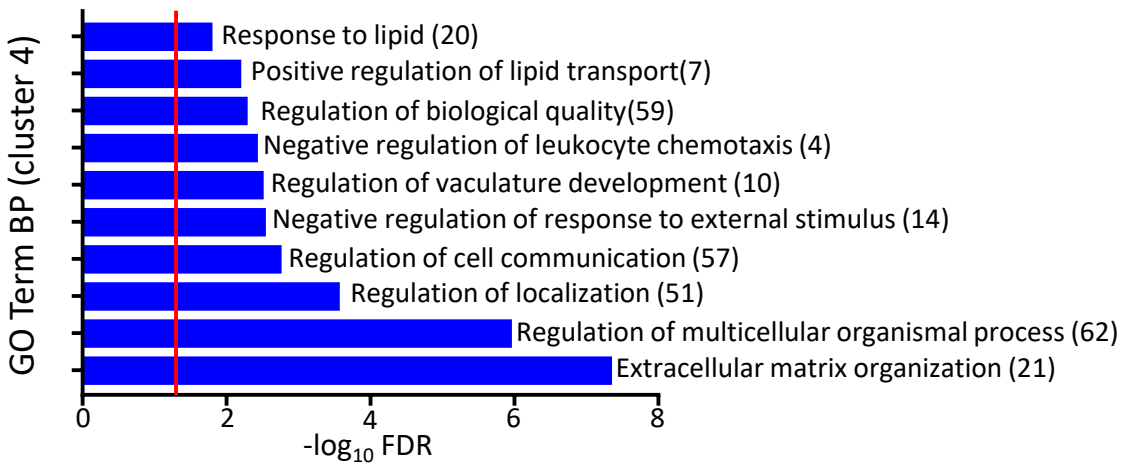

B

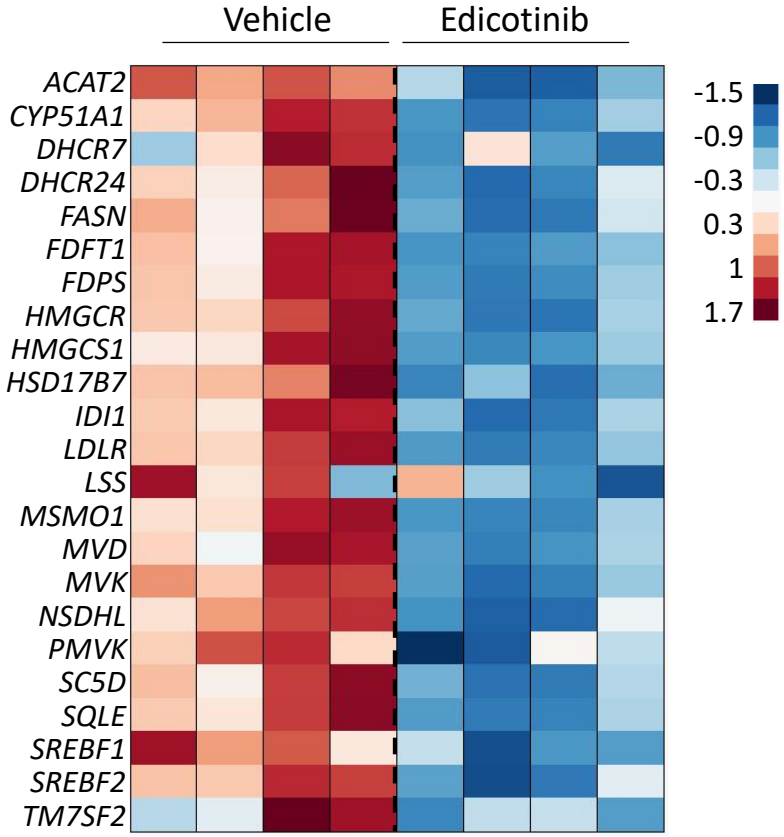

D

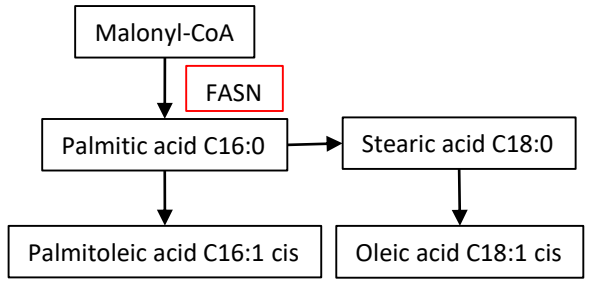

E

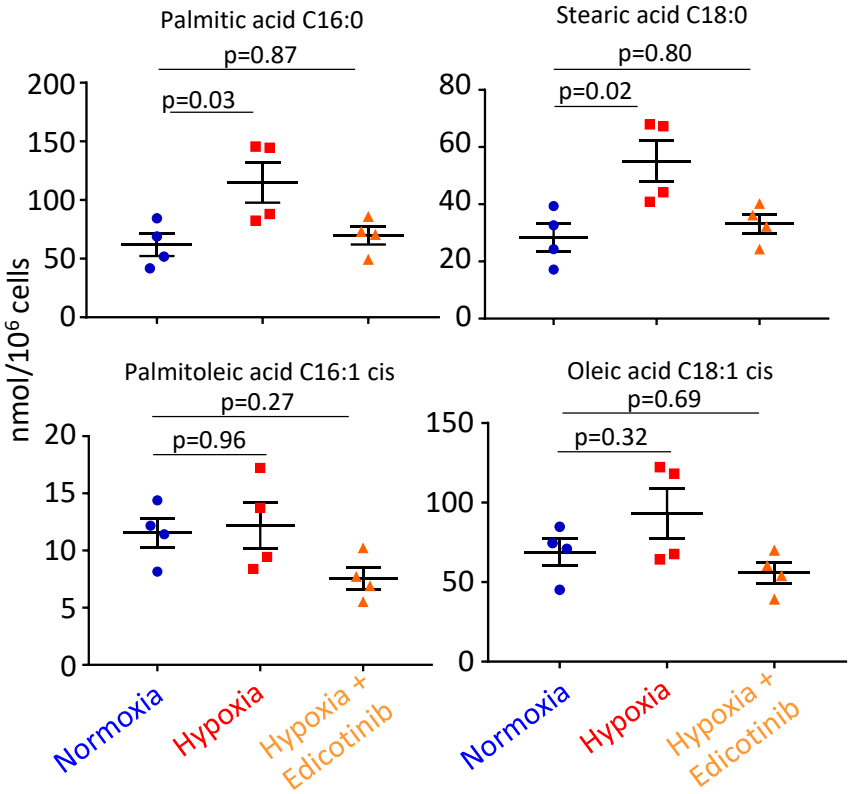

Figure 4

F

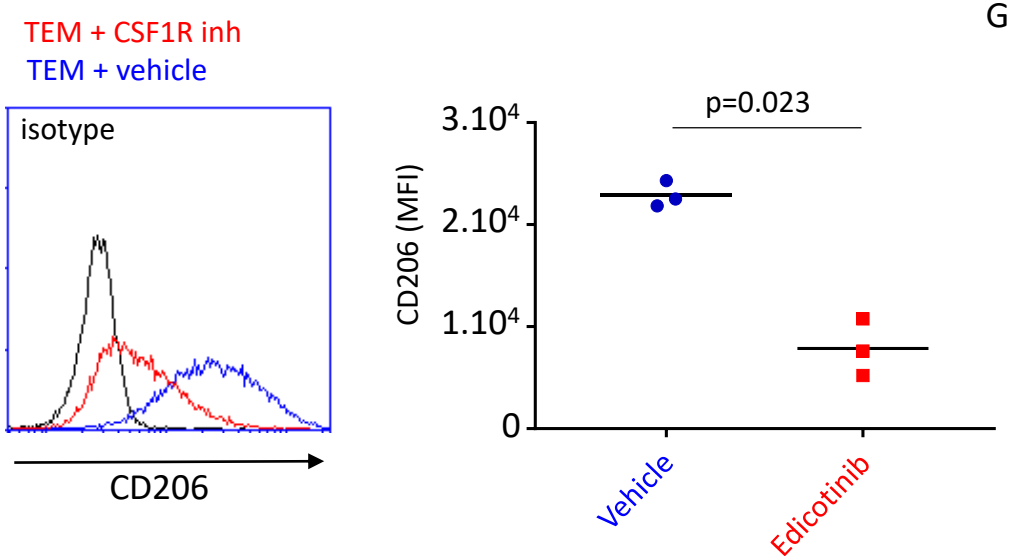
TEM + CSF1R inh
TEM + vehicle
isotype
CD206
CD206 (MFI)
3.10⁴
2.10⁴
1.10⁴
0
p=0.023
Vehicle
Edicotinib

G

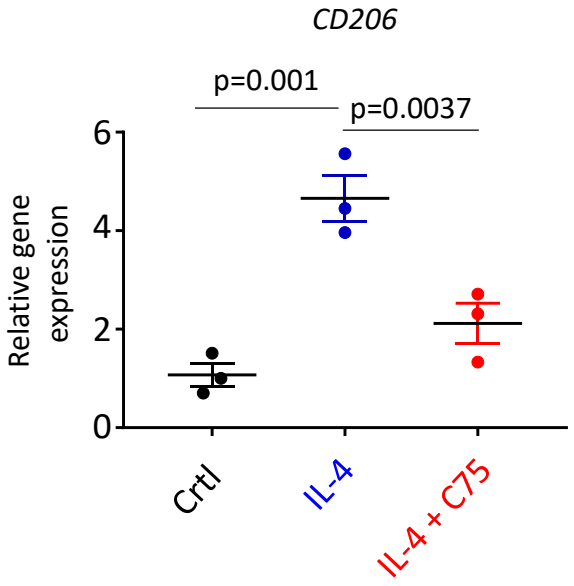
CD206
p=0.001
p=0.0037
Relative gene expression
6
4
2
0
Crtl
IL-4
IL-4 + C75

Supplemental Figure 4

A

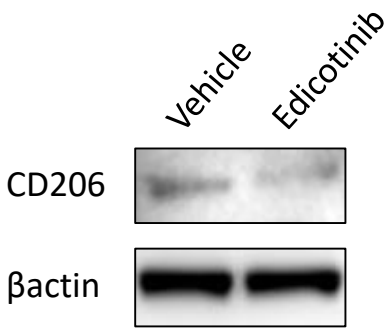

B

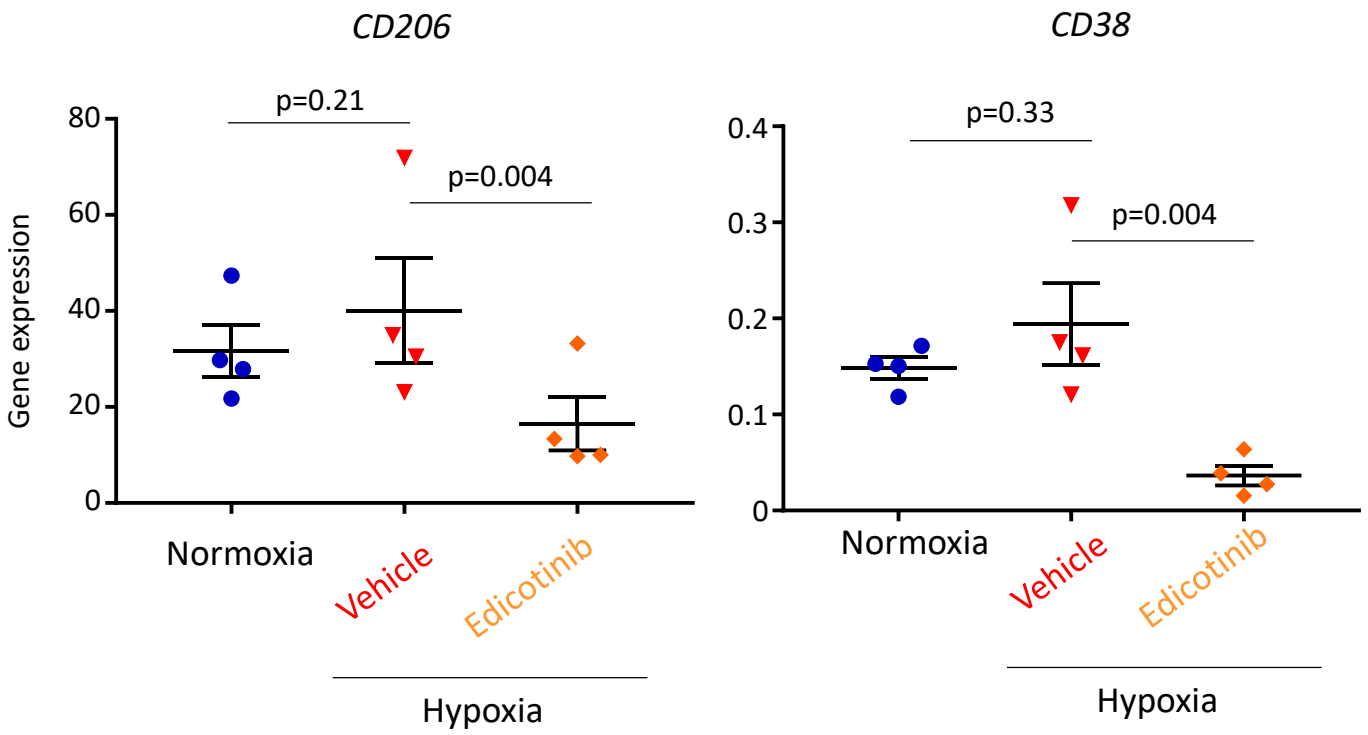

Figure 5

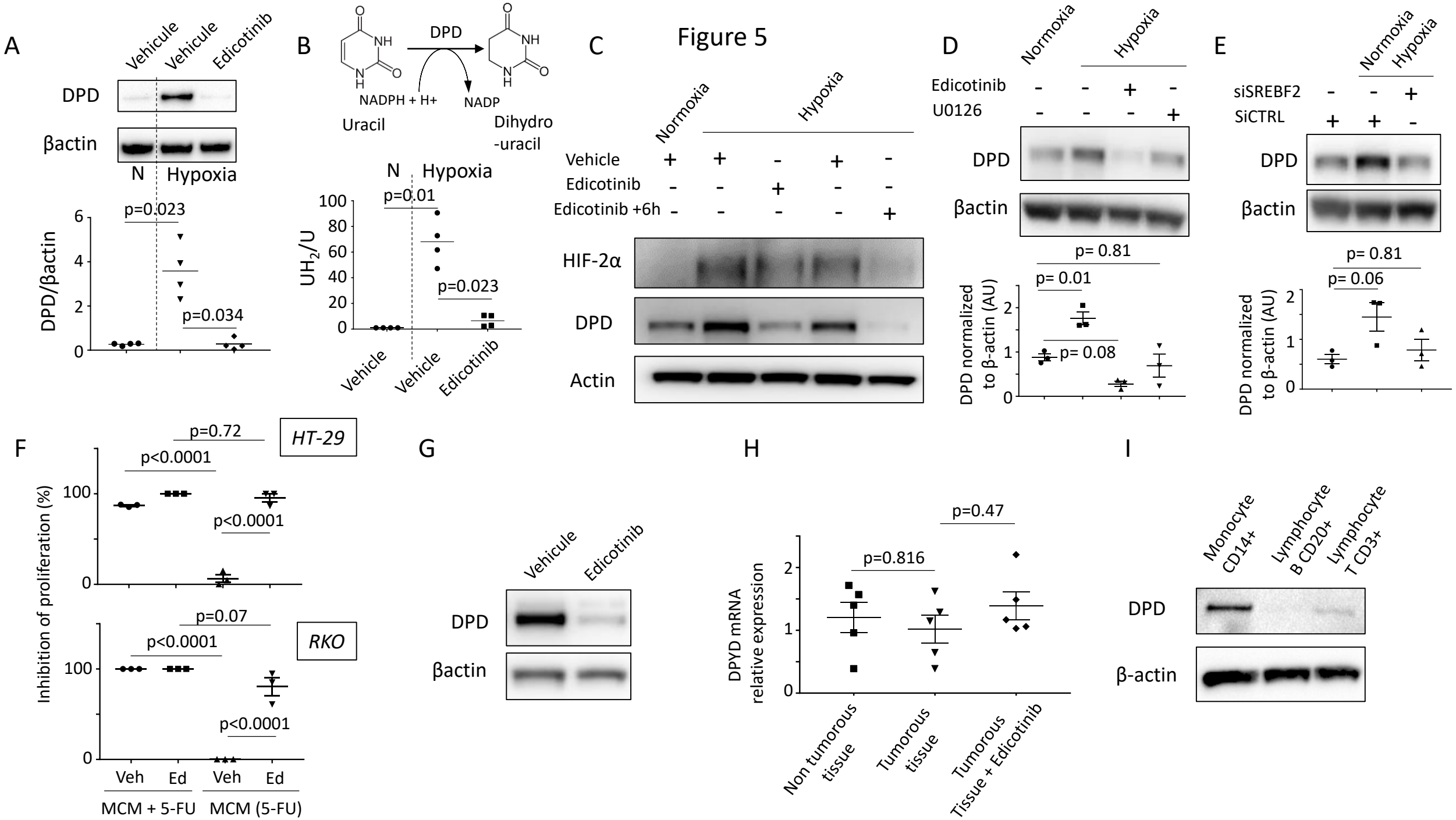
A
Vehicule
Vehicule
Edicotinib
DPD
βactin
N
Hypoxia
DPD/βactin
p=0.023
p=0.034
B
DPD
NADPH + H+
NADP
Uracil
Dihydro
-uracil
N
Hypoxia
UH2/U
p=0.01
p=0.023
Vehicle
Vehicle
Edicotinib
C
Normoxia
Hypoxia
Vehicle
Edicotinib
Edicotinib +6h
HIF-2α
DPD
Actin
D
Normoxia
Hypoxia
Edicotinib
U0126
DPD
βactin
p= 0.81
p= 0.01
p= 0.08
DPD normalized to β-actin (AU)
E
Normoxia
Hypoxia
siSREBF2
SiCTRL
DPD
βactin
p= 0.81
p= 0.06
DPD normalized to β-actin (AU)
F
HT-29
p=0.72
p<0.0001
p<0.0001
RKO
p=0.07
p<0.0001
p<0.0001
Inhibition of proliferation (%)
Veh
Ed
Veh
Ed
MCM + 5-FU
MCM (5-FU)
G
Vehicule
Edicotinib
DPD
βactin
H
p=0.47
p=0.816
DPYD mRNA relative expression
Non tumorous tissue
Tumorous tissue
Tumorous Tissue + Edicotinib
I
Monocyte CD14+
Lymphocyte B CD20+
Lymphocyte T CD3+
DPD
β-actin

Figure 5

J

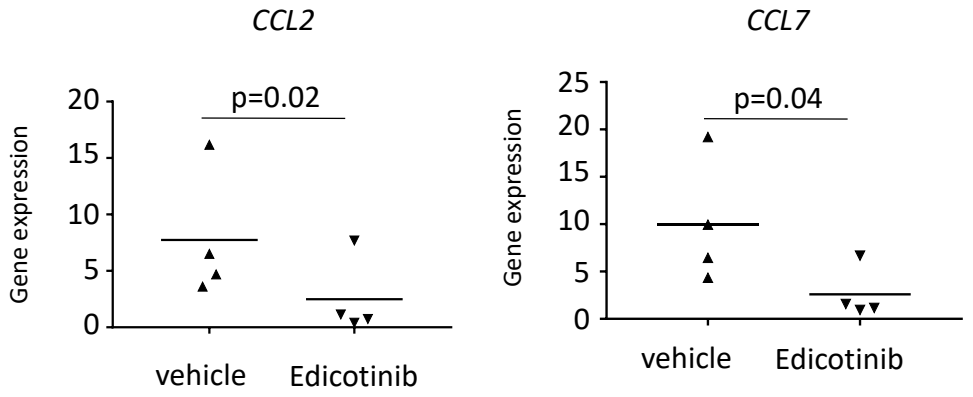
CCL2
p=0.02
Gene expression
20
15
10
5
0
vehicle
Edicotinib
CCL7
p=0.04
Gene expression
25
20
15
10
5
0
vehicle
Edicotinib

K

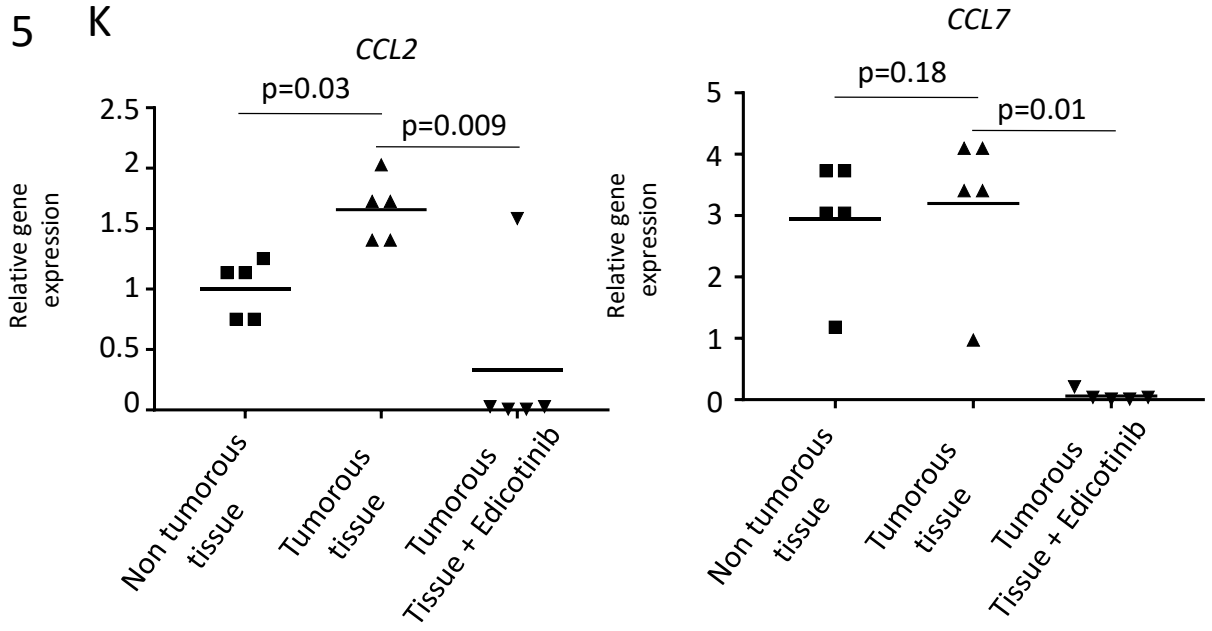
CCL2
p=0.03
p=0.009
Relative gene expression
2.5
2
1.5
1
0.5
0
Non tumorous tissue
Tumorous tissue
Tumorous Tissue + Edicotinib
CCL7
p=0.18
p=0.01
Relative gene expression
5
4
3
2
1
0
Non tumorous tissue
Tumorous tissue
Tumorous Tissue + Edicotinib

L

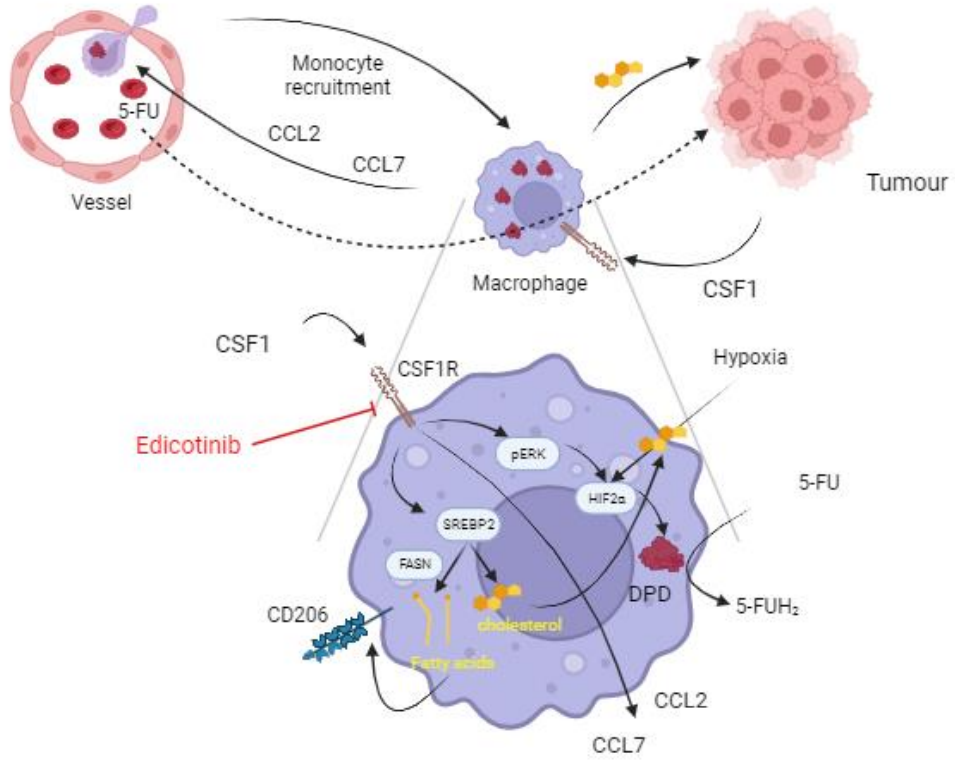
Monocyte recruitment
5-FU
CCL2
CCL7
Vessel
Tumour
Macrophage
CSF1
CSF1
CSF1R
Hypoxia
Edicotinib
pERK
HIF2α
5-FU
SREBP2
FASN
DPD
5-FUH₂
CD206
cholesterol
Fatty acids
CCL2
CCL7

Supplemental figure 5

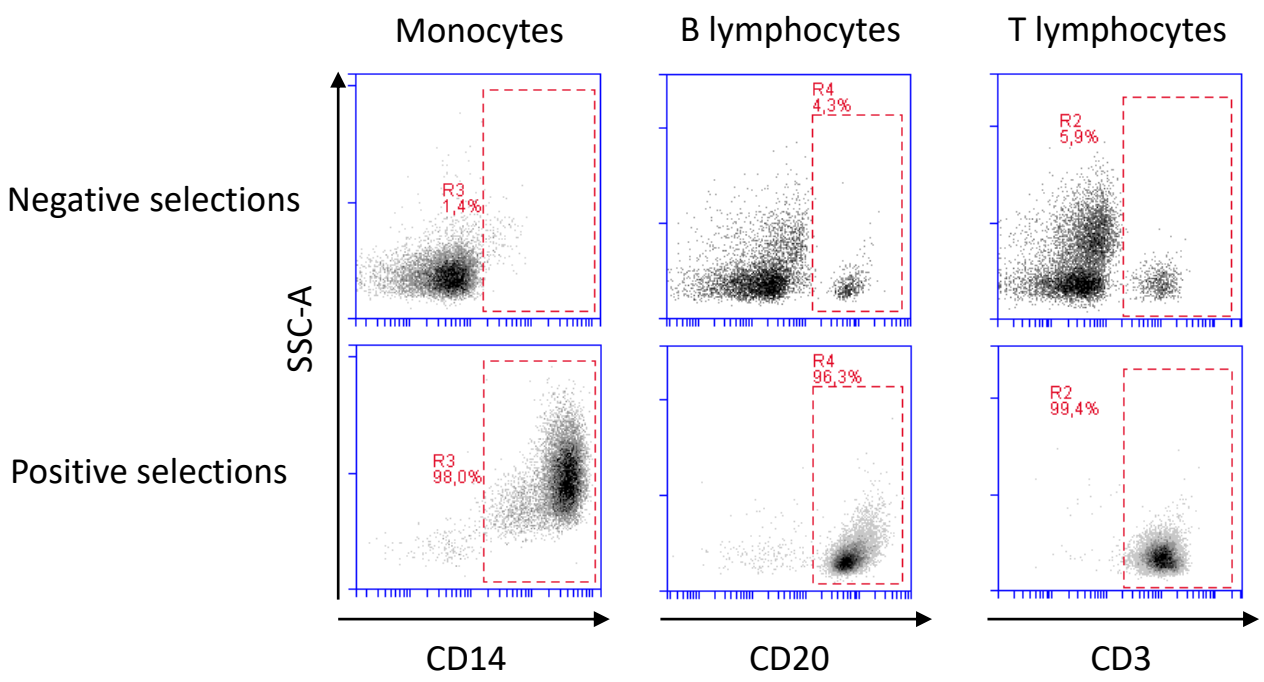

Sexe	Age	Histologic diagnosis	Surgery	TNM	Molecular charactrization
F	92	Adenocarcinoma	Right colectomy (coelioscopic)	pT4N1R0	p-MMR
M	71	Adenocarcinoma poorly differentiated	Right colectomy (coelioscopic)	pT3N1R0	MSI (loss MSH6)
F	55	Adenocarcinoma poorly differentiated low grade	Sigmoidectomy	pT3N2bR0	NA
F	69	adenocarcinoma well differnetiated on tubulovillous adenoma	Left Colectomy	pT3pN1R0	pMMR
M	74	Adenocarcinoma (lieberkühnien)	Left Colectomy	pT3N0	MSS
F	70	Adenocarcinoma (lieberkühnien) low grade	Left colectomy	pT3N0M0	MMR
M	63	Adénocarcinoma low grade	Right colectomy (coelioscopic)	pT4N1b	MMR
M	84	Adenocarcinoma (lieberkühnien) low grade	Right colectomy (coelioscopic)	pT3N0R0	NA